Received Date : 09-Oct-2010

Revised Date : 04-Oct-2011

Accepted Date : 25-Nov-2011

Article type : Original Manuscript

Aeolian construction and alluvial dismantling of a fault-bounded intracontinental aeolian dune field (Teruel Basin, Spain); a continental perspective on late Pliocene climate change and variability

JUAN PEDRO RODRÍGUEZ-LÓPEZ[1], CARLOS L. LIESA[2], JAN VAN DAM[3], PALOMA LAFUENTE[2], LUIS ARLEGUI[2], LOPE EZQUERRO[2,4], POPPE L. DE BOER[5]

[1]Grupo de Análisis de Cuencas Sedimentarias UCM-CAM. Departamento de Estratigrafía UCM. Facultad de Ciencias Geológicas. Universidad Complutense de Madrid. Ciudad Universitaria. 28040. Madrid. Spain. jprodrig@geo.ucm.es

[2]Grupo GEOTRANSFER. Área de Geodinámica interna. Departamento de Ciencias de la Tierra. Facultad de Ciencias. Universidad de Zaragoza. C/ Pedro Cerbuna, 12. 50.009. Zaragoza. Spain

[3] Institut Català de Paleontologia Miquel Crusafont, Módulo ICP, Campus de la UAB, E-08193, Cerdanyola del Vallès, Spain

[4] Área de Estratigrafía. Departamento de Ciencias de la Tierra. Facultad de Ciencias. Universidad de Zaragoza. C/ Pedro Cerbuna, 12. 50.009. Zaragoza. Spain

[5] Sedimentology Group, Department of Earth Sciences, Utrecht University, Budapestlaan 4, 3584 CD Utrecht, The Netherlands

This is an Accepted Article that has been peer-reviewed and approved for publication in the *Sedimentology,* but has yet to undergo copy-editing and proof correction. Please cite this article as an "Accepted Article"; doi: 10.1111/j.1365-3091.2011.01316.x

ABSTRACT

An aeolian dune field migrating to the east encroached on the toes of alluvial fans in the Teruel Basin (eastern Spain) during a short interval in the late Pliocene (*ca* 2.9 to 2.6 Ma), when Northern Hemisphere glaciation and strong glacial-interglacial cycles began. Preservation of the dune field was controlled by synsedimentary activity of a normal fault. Ephemeral water discharge eroded aeolian sands and formed V-shaped channels in which aeolian sandstone blocks accumulated. The incorporation of loose aeolian sand in wadi waters modified the sediment/water ratio, changing the physical properties of the flows as they penetrated the aeolian dune field. The erosion and cover of aeolian dune foresets by sheetflood deposits suggest that dune-damming caused the intermittent ponding of water behind the dunes and its flashy release. The arid climate in the late Pliocene western Mediterranean realm favoured the transport of windblown sediments from northern Africa and western Mediterranean land masses into the Mediterranean. The formation of the studied aeolian dune field (2.9 to 2.6 Ma) and possibly others (for example, the Atacama, Namib and Sahara deserts) correlates with a strong increase of the influence of obliquity, due to the combination of a regional expression of a minimum in the long-period (2.3 Ma) eccentricity and a remote expression of the onset of the Northern-Hemisphere glaciation.

Keywords: Fault-bounded aeolian dune field, alluvial fans, Pliocene climate, Northern-Hemisphere glaciation, dune field expansion, animal tracks

INTRODUCTION

Late Pliocene climate perturbations led to the establishment of a permanent Northern Hemisphere ice sheet and the onset of strong obliquity-controlled glacial–interglacial cyclicity (Shackleton et al., 1984; Ravelo *et al*., 2004; Herbert et al., 2010). Quantitative climate information from Late Pliocene European and African continental sediments is growing; for example, estimates of palaeotemperature and palaeoprecipitation based on plant and mammal records (cf. Fauquette *et al*., 1999; deMenocal, 2004; Mosbrugger *et al*., 2005; van Dam, 2006). Most data, however, come from the marine record. Astronomically tuned cyclic series from the Mediterranean (e.g. Lourens et al., 1992) show an African precession-controlled monsoon signal (for example, sapropel occurrences) and an obliquity-controlled glacial–interglacial temperature signal. Importantly, the Pliocene record in the easternmost Atlantic (Gulf of Cadiz) is dominated by a strong eccentricity-modulated precession signal related to wet–dry cycles recognized in the southern Spanish interior, with the obliquity signal showing additional importance during 100 kyr and especially 400 kyr eccentricity minima, especially in the latest Pliocene (Sierro et al., 2000).

The Pliocene aeolian sedimentary record in Europe is scarce (e.g. Ghinassi *et al*. 2004). The fault-bounded aeolian dune field system in east-central Spain allows correlating climate information from the continental realm with that from the marine realm thus providing a 'continental perspective' on Pliocene climate variability. The studied aeolian dune field is bounded by a normal fault that provided the accommodation space needed for its preservation. This paper describes and interprets the wind-laid and water-laid facies associations of the Pliocene dune field, compares this fault-bounded aeolian system with both ancient and recent counterparts and, finally, discusses the Late Cenozoic climate in the western Mediterranean from a continental perspective.

GEOLOGICAL SETTING

The Teruel Basin (Teruel Graben) in the central-eastern Iberian Chain in north-east Iberia (Fig. 1A and B) is oriented NNE–SSW, transverse to the NW–SE main structural trend of the Iberian Chain (Capote *et al.*, 2002; Liesa & Simón, 2009; Fig. 1A). It was formed during the Miocene–Pliocene rifting stage that affected the eastern margin of Iberia and formed the Valencia Trough (Gautier *et al.*, 1972; Vegas *et al.*, 1979; Álvaro *et al.*, 1979; Simón, 1982, 1983; Roca & Guimerà, 1992, among others). It generally shows a half-graben structure (Fig. 1C, E and F), defined by north–south to NNE–SSW faults along its eastern boundary (faults of the Sierra del Pobo and Teruel-Ademuz). The basin is filled by a rather complete Neogene succession up to 500 m thick (Moissenet, 1983, 1989).

The infill of the basin in the northern sector (north of Teruel), where the studied area is located (Fig. 1B), began during the earliest Late Miocene (Simón, 1983; Simón & Paricio, 1988, Alcalá *et al.*, 2000; Alonso & Calvo, 2000; Van Dam et al., 2001). In this area, the Neogene sedimentary record, tilted toward the east (towards the north–south to NNE–SSW faults of the Sierra del Pobo), comprises four stratigraphic units (Peral, Alfambra, Tortajada and Escorihuela Formations; van de Weerd, 1976). These units range from the Late Miocene (Vallesian) to the Late Pliocene (Villafranchian), and mainly represent endorheic alluvial, palustrine and lacustrine facies (van de Weerd, 1976; Anadón & Moissenet, 1996; Alcalá *et al.*, 2000; Alonso-Zarza & Calvo, 2000; Lafuente *et al*., 2008). This record has been also divided into informal (Godoy *et al.*, 1983; Anadón *et al.*, 1990) or genetic units (Alonso-Zarza and Calvo, 2000; Alcalá *et al.*, 2000).

This work deals with the Escorihuela Formation (van de Weerd, 1976), a 30 to 35 m thick succession of mainly brown sands, grey clays and white limestone beds. This unit correlates laterally with unit 'Rojo 3' of Godoy *et al*. (1983), the Perales red detrital unit of Anadón *et al.* (1990), and unit V of Alcalá *et al.* (2000) and Alonso-Zarza *et al.* (2002). It rests on the lacustrine limestones of the Alfambra Formation (upper part of unit IV of Alonso-Zarza and

Calvo, 2000 and Alcalá *et al.*, 2000) (Fig. 1D). The Escorihuela Formation is Middle–Late Pliocene to Early Pleistocene: site ESAB (Fig. 2A) correlates with European mammal unit MN15 and with the local *Dolomys* zone (van de Weerd, 1976; Mein et al., 1990; van Dam et al., 2006) whereas the stratigraphically slightly higher sites ESA, ESAA and ESAC correlate to the younger MN16 and the local *Mimomys gracilis – M. hajnackensis* Zone. A magnetostratigraphic study of the Escorihuela section (Opdyke et al., 1997, re-interpreted by Oms et al., 1999) shows the presence of the C2An.2r-C2An.2n boundary (3.2 Ma) in the lower part of the section (within the Alfambra Formation), whereas the top of the section just contains the C2An-C2r boundary (2.58 Ma). Assuming a constant sedimentation rate, these constraints imply an age of 3.05 Ma for the base of the Escorihuela Formation and an age of 2.9 to 2.6 Ma for the studied aeolian interval. The Escorihuela Formation is covered by Pleistocene (pediment) gravel deposits (Figs 1D and 2A) sourced from the Sierra del Pobo highland, in which three levels of glacis-terrace systems (cf. Hitchcock, 1860) developed during the Quaternary (Gutiérrez & Peña, 1976). This manuscript focuses on the upper part of the Escorihuela Formation, which is characterized by fine-grained to coarse-grained well-sorted sandstones and interbedded conglomerates (Fig. 2A and B) (Gutiérrez & Peña, 1976; Moissenet, 1977; Carrillo & Gisbert, 1979). It crops out in natural slopes and especially in some quarries (Fig. 2C) along the eastern bank of the Alfambra River, 2 km south of Escorihuela village (Fig. 1B and F). Five stratigraphic sections (sections E1 to E5 in Fig. 1F) have been studied in detail. The main characteristics of water-related and wind-related facies associations are summarized in Table 1.

WIND-RELATED FACIES ASSOCIATIONS

Aeolian dune deposits

Description

This facies association is formed by pale to yellow, fine to coarse-grained sandstones (Figs 2B, 3 and 4). These sandstones constitute tabular and laterally continuous bodies internally arranged in a variety of medium to large-scale trough cross-bedded sets that can be followed laterally over tens of metres, showing a clear surface hierarchy (Fig. 3A, 3B and 4A to C). Foresets display concave-up and downwind dipping surfaces (marked 'R' on Figs 3B and 4C; and marked 'S' on Fig. 4B). In detail, toesets of cross-bedding show wedges of very well-sorted, medium- to coarse-grained sands ('gf' in Fig. 4D and E) that pinch out into fine-grained, finely laminated sandstones with scattered coarse grains ('wr' in Fig. 4D and E). The upper surfaces of this facies association range from flat-sharp (as shown in Fig. 4A) to erosional-sharp (Fig. 3C). Locally, this facies association pinches out in muddy and silty tabular deposits (Fig. 3A to C). Palaeowinds were from west to east (Fig. 2D).

Interpretation

The large to medium-scale sets of trough-cross strata consisting of very well-sorted sandstones with bimodal grain-size distribution are interpreted as aeolian dune sandstones (e.g. Kocurek, 1996; Mountney, 2006a,b). These aeolian dunes display the typical hierarchy of aeolian bounding surfaces described by Brookfield (1977) and Kocurek (1981) that form by a variety of depositional processes (e.g. Mountney, 2006a). The downwind dipping concave-up surfaces (marked 'S' in Fig. 4B) resemble the superimposition surfaces described by Mountney (2006b) in the Cedar Mesa Sandstone (USA), by Scherer (2000) in the Cretaceous Botucatu Formation (Brazil) and by Rodríguez-López *et al.* (2008; 2011) in the Cretaceous Iberian erg (Spain). In all these cases superimposition surfaces are non-parallel to the cross-strata (Kocurek, 1996); they

are covered by downlapping cross-bedded sets (Mountney & Thompson, 2002; Rodríguez-López et al., 2008). These superimposition surfaces may have formed by the migration of scour troughs on the lee slope of a bedform or by the migration of superimposed dunes over a larger parent bedform (Mountney, 2006a). The downwind tabular intervals between superimposed sets (marked '1' and '2' in Fig. 4B) are interpreted as the toeset of the overlying superimposed set or as wind ripple intervals due to changes in wind regime. The downwind concave up surfaces marked 'R' (Figs 3B and 4C) developed in aeolian dune foresets, are interpreted as reactivation surfaces (cf. Mountney & Thompsom, 2002). These surfaces can be formed by a variety of processes acting over the aeolian dune foreset including changes in the direction of bedform migration, foreset reworking due to changing wind directions (Kocurek, 1981; Mountney, 2006a and references therein), and/or processes associated to changes in the asymmetry and/or steepness of the aeolian dune (Mountney, 2006a). The very well-sorted coarse-grained sand wedges merging with fine-grained very well-sorted sands are interpreted as grain flow deposits ('gf' in Fig. 4D and E) merging with wind ripple deposits ('wr' in Fig. 4D and E; cf. Hunter, 1977; Mountney, 2006b).

Aeolian sandsheet deposits

Description

This facies association forms metre-thick tabular intervals internally arranged in laterally continuous, finely laminated sandstones with a variety of sedimentary structures (Fig. 5A). In detail, intervals formed by stacked centimetre-thick lamina with inverse grading and cemented layers are interbedded with bimodal deposits of fine-grained, very well-sorted sands and very well-rounded and frosted coarse-grained sandstones and granules (Fig. 5B). These bimodal deposits are locally topped by a layer of granules, which are similar to the coarse fraction of the underlying bimodal deposits. This facies association is also characterized by intervals of subcritically climbing translatent strata showing pin-stripe lamination and inverse grading (Fig.

5C). Lamination can be followed laterally over several metres (Fig. 5A). Very often, subcritically climbing translatent strata are interbedded with ripple forms with a coarser crest formed by a very well-rounded and very well-sorted population of frosted coarse grains (Fig. 5D). Internal ripple lamination is preserved and shows alternating coarse-grained and fine-grained layers. The external ripple form displays form discordance with respect to the internal lamination (Fig. 5D). Occasionally this facies association displays tabular intervals of adhesion ripples characterized by crinkly foresets (Fig. 5E) interbedded with subcritically climbing translatent strata. Fine-grained yellowish sands are occasionally disrupted by calcitized bioturbation tubes and calcitized concretions (Fig. 5A).

Interpretation

The thick intervals of fine-grained very well-sorted finely laminated sandstones formed by subcritically climbing translatent strata have been interpreted as aeolian sandsheet deposits mainly constructed by migrating wind ripples (cf. Hunter, 1977; Fryberger *et al*., 1983; Fryberger & Schenk, 1988; Scherer *et al*., 2007). Inverse grading and pin-stripe lamination are typical for aeolian climbing translatent strata (Hunter, 1977; see fig. 7B of Clemmensen & Abrahamsen, 1983).

The ripple forms with coarse grains on preserved ripple crests and with well-sorted coarse and fine layers within the foresets (Fig. 5D) are very similar to the aeolian granule ripples described by Fryberger *et al.* (1992). Aeolian granule ripples appear interbedded with subcritically climbing translatent strata that could be formed during periods when more fine windblown sand passed across the sandsheet surface (e.g. Fryberger *et al*., 1992). Aeolian granule ripples are similar to those described by Clemmensen & Abrahamsen (1983) in the Permian Arran Basin (Scotland). The flat and discrete layers of granules and coarse sand accumulations with excellent sorting (Fig 5B) resemble the deflation lags of Clemmensen & Abrahamsen (1983). The armouring has been ascribed to long-lasting deflation of the underlying bimodal deposits, and prevented erosion of the underlying sediments (c.f. Cooke *et*

al., 1993; Rodríguez-López *et al*., 2010). The occasional occurrence of calcitized root horizons (Fig 5A) suggests periods of reduced aeolian input and surface stabilization. The adhesion ripples (Fig. 5E) indicate that during their formation the water content ranged from saturated to a saturation level just below 80% (Kocurek & Fielder, 1982). Thus, the adhesion ripples indicate that a dry sand source and a wet/damp depositional area existed simultaneously (Kocurek & Fielder, 1982).

Low-angle aeolian deposits

Description

This facies association is formed by layers dipping ≤15º (Fig. 6A); they are interbedded very well-sorted coarse-grained or granule sandstones and very well-sorted fine-grained sandstone layers internally organized in superimposed subcritically climbing translatent strata. In detail, this facies association displays discrete laminae of one grain thick, uniformly spaced, rounded grains (coarse sand and granules) aligned parallel to the lamination (Figs 6B and C). This facies association displays bimodal deposits like those observed in the aeolian sandsheet facies association. Locally, granule accumulations (Fig. 6D) are interbedded with wind ripple deposits.

Interpretation

This facies association is interpreted as a low-angle aeolian deposit similar to those described by Fryberger *et al*. (1992) and Kocurek (1986) as low-angle aeolian strata with an initial dip of 20º (Fryberger *et al*., 1992) or ≤15º (Kocurek, 1986). Similar aeolian bimodal deposits to those observed in Fig. 6B to D were described by Maxwell & Haynes (2001) in Quaternary aeolian sandsheets in Egypt. The widespread occurrence of subcritically climbing translatent strata suggests deposition due to wind ripple migration (cf. Hunter, 1977). The single-grain laminae in low-angle aeolian deposits (Fig. 6B and C) are very similar to granule lags (also named granule-rich horizons, granule veneers and granule linings; Rodríguez-López *et al*., 2010) that often

develop by deflation of dry interdune and aeolian sandsheet depositional surfaces (cf. Clemmensen & Abrahamsen, 1983; Kocurek & Nielson, 1986). The granule pavement of Fig. 6D formed due to deflation of bimodal low-angle aeolian deposits preserved below.

WATER-RELATED FACIES ASSOCIATIONS

Intraformational sandstone-conglomerate channel fill

Description

This facies association is formed by sub-rounded to sub-angular, cobble to boulder size (9 to 57 cm) sandstone clasts filling ribbon-like channel incisions in aeolian sandsheet deposits (Fig. 7A and B). The conglomerate is disorganized, lacking both internal sedimentary structures and spatial clast size organisation. No specific clast orientation is observed. Cobbles and boulders consist of fine-grained, very well-sorted sandstone with well-preserved internal lamination (Fig. 7C and D). Sandstone blocks are mixed with extraformational pebbles. The conglomerate ranges from clast- to matrix-supported and the matrix is formed by fine-grained very well-sorted sand, similar to the sandstone of the conglomerate clasts. Channels have a tight profile with near-vertical banks (Fig. 7E and F) that truncate the horizontal to sub-horizontal lamination of the aeolian sandsheets in which the channel is encased. The top of the channel fill is covered by flat-lying extraformational conglomerates and aeolian sandsheet deposits (Fig. 7A and B).

Interpretation

The fine-grained, very well-sorted sandstone forming the cobbles and boulders has the same composition as the aeolian sand in which the channel is encased. Thus, the sandstone clasts are reworked aeolian deposits that preserved the original sedimentary structures (wind-ripple lamination). The occurrence of aeolian sandstone clasts in channel deposits requires some degree of competence of the aeolian deposits, for example, due to previous wetting of aeolian

sands (Mountney & Howell, 2000) or early cementation, and, moreover, limited, short-distance transport (e.g. Deynoux *et al*., 1989).

The occurrence of aeolian sandstone blocks in wadi channels is common in inland deserts and in marginal-marine erg/dune fields. In many cases, these aeolian clasts form due to ephemeral channel bank failure (e.g. Mountney & Howell, 2000) delivering aeolian sandstone clasts to the wadi floor (Deynoux *et al*., 1989). Steep-sided wadis with even overhanging channel banks are often seen in dry areas and have been ascribed to sapping and subsurface wash (cf. Berry, 1970; Higgins, 1982); they are prone to bank collapse (Fig. 7A and B). The extraformational pebbles between the aeolian sandstone blocks indicate that the flows which eroded the aeolian deposits also transported clasts from the nearby highlands.

Debris flow deposits

Description

This facies association is formed by pebble-boulder, clast to matrix-supported, disorganized to poorly organized conglomerates (Fig. 8A) with a matrix of poorly sorted sand with floating granules, pebbles, and cobbles. Clasts are angular to subrounded limestone pebbles to boulders sourced from the adjacent Sierra del Pobo Range. This facies association is organized in 40 to 50 cm thick tabular conglomerate intervals with sharp and flat (locally slightly erosive) bases, sharp-flat to gradual tops (Fig. 8A), crude inverse grading at the base of the beds and large protruding boulders at the top. Sharp transitions in grain size occur locally (Fig. 8A). Sandstone intervals with floating clasts (granule-cobbles) and crude lamination are interbedded within the conglomerates. Certain elongated clasts are crudely imbricated, some are parallel aligned, and others are oriented vertically. There are quick lateral transitions between sand pockets with floating clasts and conglomerate zones within single units (Fig. 8A).

Interpretation

The poorly sorted tabular conglomerates with generally non-erosive bases, inverse grading and large protruding clasts are interpreted as debris flow deposits (e.g. Chamyal *et al*., 1997; Nemec & Steel, 1984). The sharp-flat base with inverse grading is indicative of a basal shear zone (Nemec & Steel, 1984). The generally clast-supported texture with locally inverse grading and crude imbrication suggests collision and friction between clasts during transport (Sohn, 2000). The crude internal layering in the conglomerates could be the product of stacked debris inter-surges alternating with debris flow surges (e.g. Nemec & Steel, 1984). The sharp lateral transitions between sandy and cobble-dominated zones could be the result of lateral flow-transition during debris flow transport (Sohn *et al*., 2002). The parallel alignment of some large clasts suggests that debris flows experienced laminar shear during emplacement (Enos, 1977). Similar vertical clasts in debris flow deposits were observed elsewhere in alluvial fans (Nemec & Steel, 1984). The sandy intervals that cover elevated and protruding boulders are interpreted as low-energy deposits produced by waning-flow traction currents after debris flow emplacement (Nemec & Steel, 1984).

Cobble-sand sheetflood deposits

Description

This facies association is formed by tabular and laterally continuous levels of conglomerates with crude cross-bedding (Fig. 8B). Conglomerates are commonly 40 cm thick and consist of carbonate clasts; they show quick lateral and vertical clast size variations. The matrix consists of fine-grained, very well-sorted sand. Strata bases are slightly erosive. The top surface is laterally continuous, sharp-flat to gradational and locally covered by pebble lags.

Interpretation

These conglomerates are interpreted as sheetflood deposits associated with alluvial fans (e.g. Turner, 1980). Carbonate clasts come from the erosion of the Sirra del Pobo Jurassic carbonates Deflation lags on top of these water-laid deposits indicate that water discharges where ephemeral and separated by deflation periods.

Boulder to sand bedload stream deposits

Description

This facies association consists of clast-supported channellized conglomerates forming metre-thick lenticular bodies encased in a variety of underlying facies associations (Fig. 8C). Lower bases are sharp and deeply erosive, and sometimes show vertical to overhanging ribbon-like channel walls (Fig. 8D). In such cases, the ribbon-like channels are filled with disorganized gravels. These conglomerates consist of angular to subangular, limestone pebbles to boulders, and display medium-scale cross-bedded sets with foreset dips near 23º, and large-scale planar cross-bedding with foreset dips near 11º. The matrix is formed by pebbly siliciclastic sandstones. Frequently the conglomerates show superimposed concave-up erosive bases (Fig. 8E). This facies association is sharply covered by aeolian deposits.

Interpretation

The lenticular conglomeratic bodies with erosive and channellized bases, sharply covered by aeolian deposits, are interpreted as streamflow deposits in ephemeral channels. The large-scale planar cross-stratified gravels result from the downstream migration of mid-channel bedforms (Fig. 8D; Chamyal *et al*., 1997). Some of the gravel foresets display characteristics similar to the transverse channel fill cross-stratification described by Ramos & Sopeña (1983). The boulder-size clasts indicate deposition by highly competent stream flows (Jo *et al*., 1997; for example, Narmada alluvial fan deposits, western India, Chamyal *et al*., 1997). Similar straight

and narrow channel fills have been described in the semi-arid Middle Souss Valley, Morocco, where Quaternary piedmont fans were fed by torrential flows (Bhiry & Occhietti, 2004). The superposition of concave-up erosion surfaces represents typical multi-storey channel-fill gravels (Fig. 8E; cf. Komatsubara, 2004).

Pebbly-sand bedload stream deposits

Description

This facies association consists of fine to coarse-grained sandstones with basal cobble lags, scattered floating pebbles and pebble pockets (Fig. 9A). Bases are sharp and erosive over the underlying aeolian deposits (Fig. 9B). Channel walls are near-vertical (Fig. 9C). The sandstones display crude horizontal lamination, planar to tangential cross-bedded sets and a clear colour contrast with the underlying yellow aeolian sandstones (Fig. 9C and D). Locally sandstones are poorly sorted, but they generally contain a very well-sorted, fine-grained population.

Interpretation

The erosive basal surface covered by a cobble lag suggests transport and erosion by channellized floods (Collinson, 1996). The infill of channels was episodic as is indicated by discrete internal erosion surfaces marked by gravel pockets (e.g. Komatsubara, 2004). The interbedding of crudely cross-bedded and flat-lying horizontal lamination suggests small dunes alternating with upper-stage plane bed sediments (Jo *et al.*, 1997 and references therein), associated with sandy bedload transport and sandy sheetfloods (cf. Blair, 1999). The gravel pockets are similar to facies C of Blair (1999) in the Anvil Spring Canyon alluvial fan (Death Valley, California), and are associated with secondary remoulding of sheetflood deposits during recessional flood stages and/or during subsequent non-catastrophic flows across the active alluvial fan lobe (Blair, 1999 and references therein). The similarity between the texture of channel fill sandstones and the underlying aeolian dunes shows that windblown deposits were

eroded by flood waters carrying extraformational clasts (e.g. Jones & Blakey, 1993; Svendsen *et al*., 2003; Rodríguez-López *et al*., 2008).

Sand–silt sheetflood deposits

Description

This facies association is formed by structureless tabular, decimetre to metre-thick intervals of muddy sandstones and siltstones (Fig. 3C). Where this facies association is interbedded with stream-flow conglomerates, it shows mottling and well-defined red and brown horizons (Fig. 8D). Locally this facies covers the erosional relief of aeolian deposits (Fig. 3C).

Interpretation

The structureless muddy sandstones were deposited rapidly with insufficient time for clast-size segregation. In combination with the widespread and well-defined mottling horizons this facies association is interpreted as distal sheetflood deposits modified by pedogenetic processes (cf. Collinson, 1996; Jo *et al*., 1997).

The relief of aeolian dune foresets, produced during floods, was filled with muddy sandstones and siltstones during waning flows (Fig. 3C). Aeolian dune erosion by floods has been described extensively in the literature (e.g. Langford & Chan, 1989; Bullard & McTainsh, 2003) and normally generates sharp erosion surfaces with an associated erosional relief (Fig. 3C). Sheetflood deposits surround isolated eroded aeolian sandstone blocks.

Damp interdune deposits

Description

This facies association is formed by tabular metre-thick intervals of mixed muddy and silty deposits with laterally continuous lamination. The sand fraction of this facies association is very similar to that of the aeolian dunes. It forms drapes over aeolian dune toesets and pinches out laterally (Fig. 3A to C).

Interpretation

The similarity of the sand fraction with that of the aeolian dunes shows that these provided the sands. The high mud content and the laterally continuous lamination and stratification suggest deposition in a damp interdune that trapped wind-blown mud and sand in interdune depressions. The inter-tonguing of dune toeset deposits with interdune strata (Fig. 3C) reflects aeolian dune advance contemporarily with damp interdune sedimentation and a gradual rise of the water table (Mountney & Thompson, 2002). Similar interdune drapes over aeolian dune toesets have been observed by others (e.g. Gradziński & Jerzykiewicz, 1974; Stanistreet & Stolhofen, 2002).

Lacustrine carbonates

Description

White carbonate mudstones to wackestones with abundant gastropods, organized in metre-thick tabular strata cover an interval of locally more than 3 m (Fig. 9E). Vertical tubular structures are abundant. The micritic limestone is interbedded and merges laterally with undifferentiated aeolian sandstones. The contact with the underlying aeolian sandstones is gradual (Fig. 9E).

Interpretation

The limestones were deposited in ponds and the vertical tubular structures reflect root activity (e.g. Sanz *et al*., 1995). The interbedded aeolian sandstones indicate that arid and semi-arid conditions alternated. The gradational transition from aeolian sandstones to limestones has been observed in other carbonate ponds (e.g. Tertiary Madrid Basin, Sanz *et al*., 1995).

ANIMAL TRACKS

Description

Aeolian deposits display soft-sediment deformation throughout the studied outcrops (Figs 10 and 11); they are concentrated at discrete intervals and covered by non-deformed aeolian deposits. Locally, structures appear stacked vertically but always at discrete levels (Fig. 11A and B). Some tracks are better displayed due to differential cementation of the laminae by calcite.

Two types of structures occur: (i) bilobate structures with a mean width of 9.7 cm and a mean depth of 3.8 cm (Fig. 10A, C and D); (ii) simple structures with a mean width of 6.3 cm and a mean depth of 8 cm (Fig. 10B, E and F). Despite geometrical differences (see below) both types show common features in cross section: (i) concave-up geometry made clear by deformed pin-stripe lamination (Figs 10A to E and 11C); (ii) folded lamination (Fig. 10B and E); (iii) vertical walls (Fig. 10D); and (iv) two marginal upfolds (Figs 10B, 10C, 10E and 11C). The concavity of the structures dies out at some 10 to 20 cm below the surface. Laminae thin laterally from non-deformed zones to folded zones. Reduction in thickness is 24 to 49% as shown by the vertical lines in Fig. 10B and E. The central axis of the structures is vertical or inclined. Structures have been filled in different ways: (i) massive infilling of the structure with granules (Fig. 10B and C); and (ii) laminated sands arranged in centimetre-thick laminae with preserved pin-stripe lamination (upper part of Fig. 11C). Very often the structures display a chaotic infill with parts cemented by carbonate. Brecciated pin-stripe lamination is observed locally (Fig. 11C, lower-right).

Interpretation

Similar track remains elsewhere (e.g. Loope 1986, 2006; Fornós *et al*., 2002; Loope & Rowe, 2003) are also characterized by concave-up structures with marginal upfolds and disrupted lamination. Animal tracks in aeolian sands occur in discrete levels and are covered by non-

deformed aeolian deposits showing that animals walked over the aeolian sands repeatedly. Aeolian dune fields and ephemeral-stream floodplains are favourable sites for the preservation of vertebrate tracks (Loope, 1986). The presence of two different patterns of tracks, bilobate and simple, shows the activity of different animals. Also the dimensions show that two types of feet sank into the aeolian sand; the relatively wide bilobate tracks reflect robust animal feet and the simple ones with a deeper imprint suggest a long and thin leg. In both cases pin-stripe lamination was compressed and folded downward and, when withdrawn from the sand, marginal upfolds formed. While the general idea is that tracks in ancient aeolian deposits were made in moist sand or preserved because they were moistened immediately before burial, Loope (2006) observed dinosaur tracks in the Navajo Sandstone (Jurassic, USA) formed mostly in dry-sand. Clay-coated dune sands are also an especially suitable medium for the preservation of these tracks (e.g. Loope, 1986). When the animal leg sank in dry sand, pin-stripe lamination was downfolded and filled with material which is texturally similar to the surrounding sediments when the leg was withdrawn (Loope, 1986), as seen in Fig. 10B and E.

Figure 11C shows an animal track filled with downlapping pin-stripe lamination due to grain flows induced by the track maker when walking across the slip face of the aeolian dune (Loope, 2006, his fig. 8). Grain flow tongues are covered by later aeolian sedimentation. Brecciated pin-stripe lamination associated with vertically stacked tracks (Fig. 11C) suggests that tracks formed in a moist (Loope, 2006) or slightly cemented sandy substrate.

DISCUSSION

Depositional system and tectonic configuration

The main structure in the area is the roughly north–south trending Sierra del Pobo basin-border fault that limits the Teruel Basin from the relief of the El Pobo Range formed by Jurassic limestones (Fig. 1E). Seismites in the aeolian sands (Lafuente *et al.*, 2008) evidence fault

activity during dune field sedimentation. Moreover, contemporary tectonic activity of nearby faults (for example, the Concud Fault, Fig. 1B; Simón, 1983; Lafuente *et al.*, 2011), and the contemporary active radial extensional stress field regime (σ_1 vertical, $\sigma_2 \approx \sigma_3$) with σ_3 preferential trajectories oriented ENE–WSW inferred for this region (e.g. Simón, 1989; Liesa, 2000; Arlegui *et al.*, 2005, 2006) also are in accordance with a syn-sedimentary extensional tectonic framework. The stratigraphic architecture (Fig. 12) shows that sub-environments of the Pliocene depositional system display a clear spatial zonation associated with the tectonic configuration of the basin. The debris flow, cobble-sand and pebble-sand bedload streams and the cobble-sand and sand-silt sheetflood deposits form a narrow belt of alluvial deposits along the eastern border fault of the Teruel Basin (Figs 12 and 13). These alluvial deposits merge laterally with aeolian dunes. Carbonate clasts were derived from erosion of the nearby Jurassic relief. Water from the El Pobo Range drove alluvial transport over the north–south trending basin-border fault producing alluvial fans (Figs 12 to 14). These marginal deposits show a proximal–distal trend in which debris flow deposits accumulated in the proximal fans, the cobble-sand and pebble-sand stream deposits in the middle portion of the fans and sheetflood deposits in the distal areas. Towards the west, the alluvial fan system pinches out into the aeolian dune field sandstones which, in turn, merge laterally with carbonate ponds (Figs 12 and 14). The aeolian dune field reflects palaeowinds from the west (Figs 2D and 12) moving the dune field perpendicular to the north–south trending border-fault thus encroaching upon the associated alluvial fan relief to the east. Windblown sands probably were sourced from Triassic and Cretaceous siliciclastic rocks that broadly crop out west of the study area in the central part of the Iberian Range (Sierra de Albarracín, Fig. 1A). In this way, the aeolian sandstones of the early Triassic Buntsandstein (Soria *et al.*, 2011) and the mid-Cretaceous desert system (Rodriguez-López *et al.*, 2006) in central–eastern Spain may have sourced the very well-sorted Pliocene aeolian sands.

Comparison with ancient fault-bounded aeolian dune fields

The configuration of the Escorihuela Formation is similar to other arid to semi-arid half-graben basins where aeolian and water-laid sediments were deposited and preserved in association with an active border fault. The studied alluvial–aeolian deposits show similarities with the Devonian Orcadian Basin (Scotland; Janaway and Parnell, 1989) which was controlled by a normal fault with associated high-relief areas where alluvial fans and sandy ephemeral alluvial systems were sourced; in the inactive parts of these systems, aeolian dune fields developed and the centre of the basin was characterized by a shallow carbonate lake similar to the Pliocene one. The example studied here also displays similarities with the Triassic deposits of the Minas sub-basin (Fundy Basin, Nova Scotia; Leleu & Hartley, 2010) in which the Cobequid Fault fed alluvial fans intertonguing with ephemeral playa lakes and aeolian dunes. The Pliocene Escorihuela Formation is also similar to the Upper Oukaimeden Member (Upper Triassic Morocco), which developed in relation to the main extensional Sidi-Fars Fault that fed alluvial fans coexisting with aeolian dunes (Fabuel-Perez et al., 2009). The main difference between these two basins is that, while marine incursions occurred in the case of the Oukaimeden Member, the Teruel Basin was an endorheic basin during the Pliocene. The Palaeoproterozoic Baker Lake half-graben (Canada) also displays marginal alluvial fans associated with border faults and the development of lake systems and aeolian dunes (Rainbird *et al*., 2003; Hadlari *et al*, 2006). In the Cambrian Guaritas Group (Brazil) alluvial fans occur in a narrow belt along the border fault and aeolian dune fields developed in the extensional basin (Marconato *et al*., 2009). The Caherbla Group (Devonian, Ireland; Horne, 1975) displays a coexisting fault-sourced alluvial fan, fluvial and aeolian dune deposits, the latter encroaching the outer slopes of the fan. In the majority of the above examples, the aeolian dune fields developed and advanced along the axial direction of the rift basin. In contrast, in the Escorihuela Formation, the aeolian dune field advanced directly towards the basin–border fault encroaching onto the alluvial fan along the El Pobo Range.

Comparison with recent fault-bounded aeolian dune fields

The control of recent dune fields and their preservation by climate and sediment budget has received considerable attention, but there is little literature on the influence of local tectonics. The majority of the recent examples of aeolian dune fields in active basins differ from the Pliocene Teruel dune field. The dune field in the Pliocene basin climbed from west to east towards the north–south trending bounding fault. In the majority of the recent counterparts, aeolian dunes move parallel or slightly oblique to the main bounding fault. For instance, aeolian dune fields in the Wadi Arava depression (Arava Valley, Death Sea Transform Valley; Fig. 15A) mainly occur east of the Arava Fault (Maercklin, 2004). This structure supports the accumulation of aeolian sands on its eastern side (Maercklin, 2004; Fig. 15B). This fault-bounded aeolian dune field differs from that of the Teruel Basin in two main aspects: (i) the bounding fault is a left-lateral strike-slip fault, the Sierra del Pobo being a normal fault; and (ii) the fault plain of the Arava Fault does not feed alluvial fans; in the Arava Valley alluvial fans come from the highlands along its eastern border (Saqqa & Atallah, 2004; Fig. 15A and B); this is a main difference with the Teruel Basin Pliocene dune field which encroached directly upon the escarpment-derived alluvial fans. Despite these differences, both depositional systems display interbedding of aeolian sands with lake deposits, muddy sabkhas in the case of Wadi Arava, and shallow carbonate lakes in the Teruel Basin. Another recent aeolian dune field, partly bounded by a fault scarp, is the Coral Pink Sand Dunes in Utah, where the Sevier Fault escarpment bounds part of the aeolian dune field (Wilkins & Ford, 2007; Fig. 15C and D). The Lençóis Maranhenses National Park aeolian dune field in Brazil developed in a different climate context but displays straight boundaries that coincide with drainage patterns parallel to the Pirapemas lineament (Almeida-Filho *et al*., 2009; Fig. 15E).

Sedimentary response to climate forcing

In aeolian systems, windblown sediment input, ultimately governed by climate, controls dune development. The studied Pliocene outcrops show that during periods of active aeolian dune field construction and advance, governed by a positive aeolian sediment input, migrating transverse dunes with the typical hierarchy of aeolian bounding surfaces developed, indicating a mature organization (Fig. 4). In periods with reduced windblown sand input, deflation lags (Fig. 5B), granule linings (Fig. 6B and C) and granule ripples (Fig. 5D) formed.

The dune field moved to the east (Fig. 2D) and encroached directly over the ephemeral channels and alluvial fans that were fed from the El Pobo Range; this led to reworking of the aeolian sands by runoff (Fig. 14). Reworked aeolian sands forming the matrix of conglomerates and the deeply encased channel in aeolian deposits (Fig. 7) are a good illustration of the incursion of high-energy, ephemeral waters. In Namibia, Krapf *et al.* (2003) showed that major floods from the Koijab Fan flushed away barchans and rejuvenated a channel network leading to new areas for aeolian reworking. Also in Baluchistan, Pakistan, aeolian dunes are partly reworked by wadi floods (Fig. 15G). In the case of the Pliocene Teruel system, erosion of aeolian dune foresets by sheetfloods (Fig. 3) suggests dune-damming as a possible cause (cf. Svendsen *et al.*; 2003).

Processes in these dynamic environments act fast. For instance, large aeolian dunes had re-occupied most of the Hunkab Channel (Namibia) already one year after a flood (Krapf *et al*., 2003). Gibling (2006) indicates that a combination of high-magnitude water flows and high sediment availability may generate both deep channel incision and filling. The intraformational conglomerate channel fills in Figs 7 to 9 show examples of such processes. The preservation of aeolian sandstone blocks indicates that they were moved *en masse* when loose aeolian sand from surrounding dunes increased the sediment/fluid ratio (e.g. Jones & Blakey, 1997) and prevented collisions between aeolian sandstone blocks during the short and quick transport.

The muddy interdune deposits (Fig. 3) indicate that the water table in interdune areas was so shallow that the moist surface could capture windblown sediment. The animal tracks show that Pliocene fauna may have been intermittently attracted to flooded interdunes when drinking water was available, or they just passed by and their tracks were preserved in the moist sand.

After flooding and/or in more humid periods, a high water table favoured the colonization of dunes by plants leading to bioturbated horizons (Figs 5A and 14C). Similar recolonization occurs in the Namib Desert today, where vegetation develops in ephemeral water courses and surrounding aeolian dunes aprons (Fig. 15F). A high water table also favoured the development of adhesion ripples (Fig. 5E). Ground water moreover recharged carbonate ponds in the distal part of the system (Figs 9E and 14A).

A continental perspective on Late Pliocene climate variability in the Mediterranean realm

The studied dune field developed during the late Pliocene (2.9 to 2.6 Ma) and its accumulation and preservation was controlled by the syn-sedimentary activity of the Sierra del Pobo Fault. The interbedding of dune sandstones with wet interdune deposits and the reworking of aeolian dunes reflect the alternation of wet and dry periods. During the Late Pliocene and Pleistocene, global climate underwent significant changes with repercussions in the continental and marine realms (for example, the onset of Northern-Hemisphere glaciation and associated global climate modifications).

.The accumulation and preservation of the intracontinental aeolian dune field in Iberia (Fig. 16B and C), the aridity recognized in the Mediterranean region during Middle and late Pliocene (Fauquette *et al*., 1999; van Dam, 2006; Hernández-Fernández *et al.*, 2007; Khélifie *et al*., 2009) and the sub-desertic landscapes in southern Spain and Northern Africa indicated by pollen data (Jost *et al*., 2009) indicate that arid conditions prevailed in the western Mediterranean continental region, intermittently interrupted by wetter intervals. The long marine pollen record from Cape Blanc (offshore western African coast; Leroy & Dupont, 1994)

and pollen records offshore Spain (e.g. Fauquette et al., 1999; Fig. 16D) reflect cyclic fluctuations in vegetation and continental climate, as well as a trend towards a dryer climate after *ca* 3 Ma. The cyclic sediments in the Gulf of Cadiz (Eastern Atlantic) between 5.2 Ma and 2.6 Ma (Fig. 16E) give clues on the regional component of the orbital forcing mechanism then affecting the Western Mediterranean region (Sierro et al., 2000). Normally, precession is the dominant orbital forcing mechanism underlying the wet–dry alternations on the Iberian mainland during the Pliocene. Interestingly, the associated amplitude reduction of the precession signal in the proxy record related to the modulation by the 100 kyr and 400 kyr eccentricity cycles (Fig. 16F), does not occur at the 400 kyr eccentricity minimum at 2.8 to 2.7 Ma (Fig. 16E; Sierro et al., 2000). Instead, the expression of obliquity is relatively strong. This can be attributed to a minimum in the long 2.3 Ma eccentricity cycle, reducing precession amplitude even further, and allowing obliquity forcing to increase (see Hilgen et al., 2003).

If the Escorihuela section, based on Opdyke et al. (1997), is correctly tied to the Geomagnetic Polarity Time Scale (Fig. 2), the lower part of the aeolian succession fits to the 400 kyr eccentricity minimum at 2.9 to 2.8 Ma (Fig. 16). The uniqueness of this aeolian interval in the basin sequence corresponds in time to the climate event at 2.7 to 2.8 Ma, when obliquity-related glacial-interglacial cycles began with concomitant changes in atmospheric and ocean circulation and the onset of bipolar icesheets (Shackleton et al., 1984; Haug et al., 1999; Ravelo *et al*., 2004; Herbert et al., 2010). The increasing influence of obliquity in the western Mediterranean therefore appears to have both a regional and a remote component.

In addition, deMenocal (2004) indicated that marine records of African climate variability document a shift toward more arid conditions after 2.8 Ma, presumably linked to the low North-Atlantic sea-surface temperatures associated with the onset of the Northern Hemisphere glaciation. This change in marine deposits is associated with the above-mentioned increase in 41 ky aeolian variance (deMenocal, 2004) which persisted until *ca* 1.0 Ma, when a *ca* 100 kyr cyclicity became dominant. The aridification associated with global climate cooling in the late Pliocene, just after 3 Ma, was reported to also have been recorded in the Atacama, Sahara and

Namib Deserts (Hartley and Chong, 2002; (Van Zinderen Bakker and Mercer, 1986). This increase in continental aridification recorded in South America, Africa and the Iberian continental realm coincides with a marked increase in the climatic expression of the obliquity component in the deep marine record, as expressed in a larger amplitude of foraminifer $\delta^{18}O$ values in deep-sea sediments (deMenocal, 1995; Maslin et al., 1995, Zachos et al., 2001).

During the development of the Escorihuela dune field (2.9 to 2.6 Ma), the newly evolving late Pliocene–Pleistocene glacial–interglacial climate brought cooler winters to the Mediterranean region, leading to the replacement of flora with thermophylic elements by an alternation of glacial *Artemisia* steppes with interglacial deciduous forests (Suc et al., 1995), consistent with a decrease of temperature and precipitation (Fig. 16; Fauquette et al., 1998). Consistently, at the same time, the cold-water indicator *Neogloboquadrina atlantica* entered the Mediterranean (Lourens et al., 1992).

The Escorihuela intracontinental aeolian dune field shows evidence of alternating dry periods with wind activity and the migration and accumulation of aeolian dunes (Fig. 13), and more humid periods with water influx (Fig. 14) when aeolian dunes co-existed with lateral lacustrine units and alluvial conglomerate deposition (Fig. 12). The increased humidity is illustrated by the development of plant roots, the preservation of animal tracks in wet interdune deposits and the rise of the phreatic level making the aeolian sands more cohesive and/or leading to slight cementation. Indeed some tracks display evidence of having been made in wet aeolian dunes, as demonstrated by the brecciated pin-stripe lamination.

The climate variability shown in the continental dune field successions resembles the variability observed in the adjacent marine realms. Although it is tempting to try correlating individual dry–wet cycles to the insolation curve (see, for example, the section recorded by Opdyke et al. (1977) in Fig. 16), the spatial variability in sedimentation and preservation (cf. Fig. 12) does not allow such an assessment.

CONCLUSIONS

During the late Pliocene (2.9 to 2.6 Ma) the Teruel basin hosted a syn-rift aeolian dune field in which accumulation and preservation was controlled by the syn-sedimentary activity of the Sierra del Pobo Fault. This dune field underwent destructive periods characterized by flashy water influxes into the dune field leading to intense reworking of aeolian dunes and sandsheets. V-shaped channels encased in aeolian sandstones were filled by aeolian blocks derived from collapsing banks. The proximity of the aeolian dune field to the El Pobo Range favoured aeolian dune damming by which waters from the highlands could accumulate behind dunes followed by break-through and their partial erosion and destruction. During arid stages, aeolian dunes migrated from west to east, encroaching on the toes of alluvial fans along the El Pobo Range. In wetter periods, debris flows, streams and sheetfloods further built out the alluvial fan depositional system which pinched out the aeolian dune field. Animal tracks in aeolian deposits affected both dry and wet sand during humid stages when interdunes were recharged by ground water and flood waters. Despite the climate variability in the Pliocene aeolian dune field, arid conditions prevailed in the eastern Iberian Peninsula and westerly winds could transport windblown material to the coeval western Mediterranean. The estimated timing of the formation of the studied aeolian dune field (2.9 to 2.6 Ma) correlates with a strong and presumably regionally dry 400 kyr eccentricity minimum (2.8 to 2.7 Ma), with the onset of the Northern-Hemisphere glaciation leading to stronger westerlies, and with the expansion of other aeolian dune fields worldwide (for example, Atacama, Namib and Sahara deserts).

ACKNOWLEDGEMENTS

We are grateful to the journal editor Prof. Stephen Rice for editorial management. The authors are grateful to Dr. David B. Loope and Dr. Gonzalo Veiga for detailed reviews and useful comments and suggestions. We are grateful to Prof. Dr. J.L. Simón, Dr. M.A. Rodríguez-Pascua, and Dr. P. Alfaro for their helpful observations and interpretations during field work, and thank Dr. Frits Hilgen for discussing the expression of orbital forcing. This research is a contribution to the 'Geotransfer' research group of the Gobierno de Aragón, the 'Análisis de Cuencas Sedimentarias' Group of the UCM-CAM, and projects CGL2009-13390 and CGL2008-04518 (Spanish Ministerio de Ciencia e Innovación and FEDER) and Consolider CGL2006-041 («Topo-Iberia»).

REFERENCES

Alcalá, L. (1994): *Macromamíferos neógenos de la fosa de Alfambra-Teruel. Instituto de Estudios Turolenses-Museo Nacional de Ciencias Naturales*, Teruel, 554 pp.

Alcalá, L.., Alonso-Zarza, A., Álvarez, M.A., Azanza, B., Calvo, J.P., Cañaveras, J.C., van Dam, J.A., Garcés, M., Krijgsman, W., Meulen, A.J. van der, Morales, J., Peláez, P., Pérez-González, A., Sánchez, S., Sancho, R., and **Sanz, E,** (2000) El registro sedimentario y faunístico de las cuencas de Calatayud-Daroca y Teruel. Evolución paleoambiental y paleoclimática durante el Neógeno. *Rev. Soc. Geol. España*, **13**, 323-343.

Almeida-Filho, R., Rossetti, D.F., Miranda, F.P., Ferreira, F.J., Silva, C. and **Beisl, C.** (2009) Quaternary reactivation of a basement structure in the Barreirinhas Basin, Brazilian Equatorial Margin. *Quaternary Research,* **72**, 103-110.

Alonso-Zarza, A.M. and **Calvo, J.P. (2000)** Palustrine sedimentation in an episodically subsiding basin: the Miocene of the northern Teruel Graben (Spain). *Palaeogeography, Paleoclimatology, Palaeoecology*, **160**, 1-21.

Álvaro, M., Capote, R. and **Vegas, R.** (1979) Un modelo de evolución geotectónicapara la Cadena Celtibérica. *Acta Geol. Hisp.*, **14**, 172-177.

Anadón, P. and **Moissenet, E.** (1996) Neogene basins in the Eastern Iberian Range. In: *Tertiary basins of Spain. The stratigraphic record of crustal kinematics* (Eds. P.F. Friend & C.J. Dabrio). Cambridge Univ. Press, Cambridge, 68-76.

Anadón, P., Moissenet, E. and **Simón, J.L.** (1990) The Neogene grabens of the Eastern Iberian Chain. In: *Iberian Neogene Basins:* (Eds. J. Agustí & J. Martorell). Field guide boook, IXth R.C.M.N.S. Congress. *Paleontologia i Evolució*, Mem. Spec. 2. 98-130.

Arlegui, L.E., Simón, J.L., Lisle, R.J., and **Orife, T.** (2005) Late Pliocene-Pleistocene stress field in the Teruel and Jiloca grabens (eastern Spain): contribution of a new method of stress inversion. *Journal of Structural Geology*, **27**, 693-705.

Arlegui, L.E., Simón, J.L., Lisle, R.J., and **Orife, T.** (2006) Analysis of non-striated faults in a recent extensional setting: the Plio-Pleistocene Concud fault (Jiloca graben, eastern Spain). *Journal of Structural Geology*, **28**, 1019-1027.

Bajpai V.N., Saha Roy T.K. and **Tandon S.K.** (2001) Subsurface sediment accumulation patterns and their relationships with tectonic lineaments in the semi-arid Luni river basin, Rajasthan, Western India. *J. Arid Environ.*, **48**, 603-621.

Berry, L. (1970) Some Erosional Features due to Piping and Sub-Surface Wash with Special Reference to the Sudan. *Geografiska Annaler. Series A, Physical Geography*, 52, 113-119.

Bhiry, N. and **Occhietti, S.** (2004) Fluvial sedimentation in a semi-arid region: the fan and interfan system of the Middle Souss Valley, Morocco. *Proceedings of the Geologists' Association*, **115**, 313-324.

Blakey, R.C. (1988) Basin tectonics and erg response. *Sed. Geol.*, **56**, 127-151.

Blair, T.C. (1999) Sedimentary processes and facies of the waterlaid Anvil Spring Canyon alluvial fan, Death Valley, California. *Sedimentology*, **46**, 913-940.

Bouloubassi, I., Rullkötter, J. and **Meyers, P.A.** (1999) Origin and transformation of organic matter in Pliocene–Pleistocene Mediterranean sapropels: organic geochemical evidence reviewed. *Marine Geology*, **153**, 177–197.

Bourquin, S., Guillocheau, F. and Péron, S. (2009) Braided rivers within an arid alluvial plain (example from the Lower Triassic, western German Basin): recognition criteria and expression of stratigraphic cycles. *Sedimentology*, 56, 2235-2264.

Brookfield, M.E. (1977) The origin of bounding surfaces in ancient aeolian sandstones. *Sedimentology*, **24**, 303-332.

Bullard, J.E. and **McTainsh, G.H.** (2003) Aeolian fluvial interactions in dryland environments: examples, concepts and Australia case study. *Prog. Phys. Geogr.*, **27,** 471-501.

Capote, R., Muñoz, J.A., Simón, J.L., Liesa, C.L. and **Arlegui, L.E.** (2002) Alpine Tectonics I : The alpine system north of the Betic Cordillera. In: *The Geology of Spain* (Eds W. Gibbons and T. Moreno). The Geol. Soc. London. p. 368-400.

Carrillo, L. and **Gisbert, J.** (1979) Análisis sedimentológico de unos depósitos tipo 'wadi' en el Plio-Cuaternario de Escorihuela (Teruel). *Boletín Geológico y Minero,* **IV**, 329-332.

Chamyal, L.S., Khadkikar, A.S., Malik, J. N. and **Maurya D. M.** (1997) Sedimentology of the Narmada alluvial fan, western India. *Sed. Geol.*, **107**, 263-279.

Clemmensen, L.C. and **Abrahamsen, K.** (1983) Aeolian stratification and facies association in desert sediments, Arran basin (Permian), Scotland. *Sedimentology*, **30**, 311-339.

Collinson, J.D. (1996) Alluvial sediments. In: *Sedimentary environments* (Ed. H.G. Reading). Blackwell-Science. p. 37-82.

Cooke, R., Warren, A., Goudie, A. (1993) *Desert Geomorphology*. University College London, London. 526 pp.

deMenocal, P.B. (1995) Plio-Pleistocene African Climate. *Science*, **270**, 53-59.

deMenocal, P.B. (2004) African climate change and faunal evolution during the Pliocene-Pleistocene. *Earth and Planetary Science Letters*, 220, 3-24.

Deynoux, M., Kocurek, G. and **Proust, J.N.** (1989) Late Proterozoic periglacial aeolian deposits on the West African Platform, Taoudeni Basin, western Mali. *Sedimentology*, **36**, 531-549.

Enos, P. (1977) Flow regimes in debris flow. *Sedimentology*, **24**, 133-142.

Fabuel-Perez, I., Redfern, J. and **Hodgetts, D.** (2009) Sedimentology of an intra-montane rift-controlled fluvial dominated succession: The Upper Triassic Oukaimeden Sandstone Formation, Central High Atlas, Morocco. *Sed. Geol.*, **218**, 103-140.

Fauquette S., **Suc J.-P., Guiot J., Diniz F., Feddi N., Zheng Z., Bessais E.** and **Drivaliari A.** (1999) Climate and biomes in the West Mediterranean area during the Pliocene. *Palaeogeogr., Palaeoclimatol., Palaeoecol.,* **152**, 15-36.

Fornós, J.J., Bromley, R.G., Clemmensen, L.A. and **Rodríguez-Perea, A.** (2002) Tracks and trackways of *Myotragus balearicus* Bate (Artiodactyla, Caprinae) in Pleistocene aeolianites from Mallorca(Balearic Islands, Western Mediterranean). *Palaeogeogr., Palaeoclimatol., Palaeoecol.*, **180**, 277–313.

Foucault A. and **Mélières F.** (2000) Palaeoclimatic cyclicity in central Mediterranean Pliocene sediments: the mineralogical signal. *Palaeogeogr., Palaeoclimatol., Palaeoecol.,* **158**, 311-323.

Fryberger, S.G. (1993) A review of aeolian bounding surfaces, with examples from the Permian Minnelusa Formation, USA. In: *Characterization of fluvial and aeolian reservoirs* (Eds C.P. North and D.J. Prosser). *Geol. Soc. Am. Spec. Pap.*, **73**, pp 167-197.

Fryberger, S.G., Al-Sari, A. M., and **Clisham, T.J.** (1983) Eolian dune, interdune, sandsheet, and siliciclastic sabkha sediments of an offshore prograding sand sea, Dhahran Area, Saudi Arabia. *Am. Assoc. Petrol. Geol. Bull.*, **67**, 280-312.

Fryberger, S.G. and **Schenk, C.J.** (1988) Pin stripe lamination: a distinctive feature of modern and ancient eolian sediments. *Sed. Geol.*, **55**, 1-15.

Fryberger, S. G., Hesp, P. and **Hastings, K.** (1992) Aeolian granule ripple deposits, Namibia. *Sedimentology*, 39, 319-331.

Fujioka, T., Chappell, J., Keith Fifield, L. and **Rhodes, E.J.** (2009) Australian desert dune fields initiated with Pliocene-Pleistocene global climatic shift. *Geology*, 37, 51-54.

Gallego-Torres, D., Mart´ınez-Ruiz, F., Paytan, A., Jimenez-Espejo, F. J. and **Ortega-Huertas, M.** (2007) Pliocene-Holocene evolution of depositional conditions in the Eastern Mediterranean: role of anoxia vs. productivity at time of sapropel deposition, *Palaeogeogr. Palaeocl., Palaeoecol.*, **246**, 424–439.

Garcés, M., Krijgsman, W., van Dam, J., Calvo, J.P., Alcalá, L., and **Alonso, A.M.** (1999) Late Miocene alluvial sediments from the Teruel area: magnetostratigraphy, magnetic susceptivity, and facies organisation. *Acta Geológica Hispánica*, **32**, 171-184.

Gautier, F., Moissenet, E. and **Viallard, P.** (1972) Contribution à l'étude stratigraphique et tectonique du fossé néogène de Teruel (Chaînes Ibériques, Espagne). *Bull. Mus. Nat. D'Hist. Natur.*, 3ª, 77, Sci. Terre, **16**, 179-208.

Ghinassi, M., Magi, M., Sagri, M. and **Singer, B.S.** (2004) Arid climate 2.5 Ma in the Plio-Pleistocene Valdarno Basin (Northern Apennines, Italy). *Palaeogeogr. Palaeoclimatol. Palaeoecol.*, **207**,37-57.

Gibling, M.R. (2006) Width and Thickness of Fluvial Channel Bodies and Valley Fills in the Geological Record: A Literature Compilation and Classification. *J. Sed. Res.,* **76**, 731-770.

Godoy, A., Moissenet, E., Ramírez, J.I., Olivé, A., Aznar, J.M., Jerez Mir, L., Aragonés, E., Aguilar, M.J., Ramírez del Pozo, J., Leal, M.C., Adrover, R., Alberdi, M.T., Giner, J., Gutiérrez Elorza, M., Portero, J.M. and **Gabaldón, V.** (1983): *Mapa Geológico de España 1: 50.000, hoja nº 542 (Alfambra).* IGME, Madrid.

Gradziński, R. and **Jerzykiewicz, T.** (1974) Dinosaur- and mammal-bearing aeolian and associated deposits of the Upper Cretaceous in the Gobi Desert (Mongolia). *Sed. Geol.*, **12**, 249-278.

Gutiérrez, M. and **Peña, J.L.** (1976) Glacis y terrazas en el curso medio del río Alfambra (provincia de Teruel). *Bol. Geol. y Min.*, **87**, 561-570.

Hadlari, T., Rainbird, R.H. and **Donaldson, J. A.** (2006) Alluvial, eolian and lacustrine sedimentology of a Paleoproterozoic half-graben, Baker Lake Basin, Nunavut, Canada *Sed. Geol.*, **190**, 47-70.

Hartley, A.J. and **Chong, G.** (2002) Late PLiocene age for the Atacama Desert: Implications for desertification of western South America. *Geology*, **30**, 43-46.

Higgins, C.G. (1982) Drainage systems developed by sapping on Earth and Mars. *Geology*, 10, 147-152.

Hilgen, F.J. (1991) Extension of the astronomically calibrated (polarity) time scale to the Miocene-Pliocene boundary. *Earth and Planet. Scien. Lett.*, **107**, 349–368.

Hitchcock, E. (1860) *Illustrations of surface geology*. J.S. & C. Adams, Amherst, 155 pp.

Hernández Fernández, M., Álvarez Sierra, M.A., and **Peláez-Camponanes, P.** (2007) Bioclimatic analysis of rodent palaeofaunas reveals severe climatic changes in Southwestern Europe during the Plio-Pleistocene. *Palaeogeogr. Palaeoclimatol. Palaeoecol.,* **251**, 500–526.

Horne, R.R. (1975) The association of alluvial fan, aeolian and fluviatile facies in the Caherbla Group (Devonian), Dingle Peninsula, Ireland. *J. Sed. Res.,* **45**, 535-540.

Hunter, R.E. (1977) Basic types of stratification in small eolian dunes. *Sedimentology*, **24**, 361-387.

Jo, H.R., Rhee, C.W. and **Chough, S.K.** (1997) Distinctive characteristics of a streamflow-dominated alluvial fan deposit: Sanghori area, Kyongsang Basin (Early Cretaceous), southeastern Korea. *Sed. Geol.*, **110**, 51-59.

Jones, L.S. and **Blakey, R.C.** (1993) Erosional remnants and adjacent unconformities along an eolian-marine boundary of the Page Sandstone and Carmel Formation, middle Jurassic, south-central Utah. *J. Sed. Petrol.*, **63**, 852-859.

Jost, A., Fauquette, S., Kageyama, M., Krinner, G., Ramstein, G., Suc J.P. and **Violette, S.** (2009) High resolution climate and vegetation simulations of the Late Pliocene, a model-data comparison over western Europe and the Mediterranean region. *Climate of the Past*, **5**, 585-606.

Khélifi. N., Sarnthein., M., Andersen, N., Blanz, T., Frank, M., Garbe-Schönberg, D., Haley, B.A., Stumpf, R. and **Weinelt**, **M.** (2009) A major and long-term Pliocene intensification of the Mediterranean outflow, 3.5–3.3 Ma ago. *Geology,* **37***,* 811-814.

Knight, J. (2008) The environmental significance of ventifacts: A critical review. *Earth-Sci. Rev.*, **86**, 89-105.

Kocurek, G. (1981) Significance of interdune deposits and bounding surfaces in aeolian dune sands. *Sedimentology*, **28**, 753-780.

Kocurek, G. (1986) Origins of low-angle stratification in aeolian deposits. In: *Aeolian Geomorphology* (Ed W.G. Nickling) *Proceedings of the 17th Annual Binghamton Symposium*. Allen & Unwin, pp. 177-193.

Kocurek, G. (1996) Desert aeolian systems. In: *Sedimentary Environments: Processes, Facies and Stratigraphy* (Ed. H.G. Reading) 3rd ed, pp. 125-153. Blackwell-Science, Oxford.

Kocurek, G. and **Havholm, K.G.** (1993) Eolian Sequence Stratigraphy--A Conceptual Framework. In: *Siliciclastic Sequence Stratigraphy: Recent Developments and Applications* (Eds. P. Weimer, H.W. Posamentier). AAPG Memoir, **58**, p. 393-409

Kocurek, G. and **Fielder, G.** (1982) Adhesion structures. *J. Sed. Res.,* **52**, 1229-1241.

Kocurek, G. and **Nielson, J.** (1986) Conditions favourable for the formation of warm-climate aeolian sandsheets. *Sedimentology*, **33,** 795-816.

Komatsubara, J. (2004) Fluvial architecture and sequence stratigraphy of the Eocene to Oligocene Iwaki Formation, northeast Japan: channel-fills related to the sea-level change. *Sed. Geol.*, **168**, 109–123.

Krapf, C.B.E., Stollhofen, H. and **Stanistreet, I.G.** (2003) Contrasting styles of ephemeral river systems and their interaction with dunes of the Skeleton Coast erg (Namibia) *Quat. Int.*, **104**, 41-52.

Lafuente, P., Arlegui, L.E., Liesa, C.L., and **Simón, J.L.** (2010) Paleoseismological analysis of an intraplate extensional structure: the Concud fault (Iberian Chain, eastern Spain). *Int. J. Earth Sci.* (*Geol. Rundsch*.). DOI 10.1007/s00531-010-0542-1.

Lafuente, P., Rodríguez-Pascua, M.A., Simón, J.L., Arlegui, L.E., and **Liesa, C.L.** (2008) Sismitas en depósitos pliocenos y pleistocenos de la fosa de Teruel. *Rev. Soc. Geol. España*, **21**, 133-149.

Langford, R.P. and **Chan, M.A.** (1989) Fluvial-aeolian interactions: Part II, ancient systems. *Sedimentology*, **36**, 1037-1051.

Larrasoaña, J.C., Roberts, A.P., Stoner, J.S., Richter, C. and **Wehausen, R.** (2003) A new proxy for bottom-water ventilation in the eastern Mediterranean based on diagenetically controlled magnetic properties of sapropel-bearing sediments. *Palaeogeogr. Palaeoclimatol. Palaeoecol.,* **190**, 221–242.

Leleu, S. and **Hartley, A.J.** (2010) Controls on the stratigraphic development of the Triassic Fundy Basin, Nova Scotia: implications for the tectonostratigraphic evolution of Triassic Atlantic rift basins. *J. Geol. Soc. London*, **167**, 437-454.

Leroy S. and **Dupont, L.** (1994) Development of vegetation and continental aridity in northwestern Africa during the Late Pliocene: the pollen record of ODP site 658. *Palaeogeogr., Palaeoclimatol., Palaeoecol., **109***, 295-316.

Liesa, C.L. (2000) Fracturación y campos de esfuerzos compresivos alpinos en la Cordillera Ibérica y el NE peninsular. Ph. D. Thesis, Universidad de Zaragoza, Spain, 760 pp.

Liesa, C.L. and **Simón, J.L.** (2009) Evolution of intraplate stress fields under multiple compressions: The case of the Iberian Chain (NE Spain). *Tectonophysics*, doi: 10.1016/j.tecto.2009.02.002.

Loope, D.B. (1986) Recognizing and utilizing vertebrate tracks in cross section: Cenozoic hoofprints from Nebraska. *Palaios*, **1**, 141-151.

Loope, D.B. (2006) Dry-Season Tracks in dinosaur-triggered grainflows. *Palaios*, **21**, 132-142.

Loope, D.B. and **Rowe, C.M.** (2003) Long-lived pluvial episodes during deposition of the Navajo Sandstone. *The Journal of Geology*, **111**, 223-232.

Lourens, L., Hilgen, F., Shackleton, N.J., Laskar, J., Wilson, D., 2004. The Neogene Period. In: Gradstein, F.M., Ogg, J.G., Smith, A.G. (Eds.), A geologic time scale 2004. Cambridge University Press, Cambridge, pp. 409–440.

Maerscklin, N. (2004) *Seismic structure of the Arava Fault, Dead Sea Transform*. Ph. D. Thesis. University of Postdam, Germany, 141 pp.

Marconato, A., Almeida, R.P., Santos, M.G.M., Nóbrega, J.E.S. and **Souza, R.B.** (2009) Alluvial-eolian Interaction in a Cambrian Rift Margin: The Pedra Das Torrinhas and Pedra Pintada Formations (Guaritas Group, RS). *Anais da Academia Brasileira de Ciências,* **81**, 819-836.

Marzo, **M**. (1986) Secuencias fluvio-eólicas en el Buntsandstein del macizo de Garraf (provincia de Barcelona). *Cuadernos de Geología Ibérica,* **10**, 207-233.

Maxwell, T.A. and **Haynes, Jr.C.V.** (2001) Sand sheet dynamics and Quaternary landscape evolution of the Selima Sand Sheet, southern Egypt. *Quaternary Science Reviews*, **20**, 1623-1647.

Moissenet, E. (1977) L'evolution Néogene de quelques basins continentaux de la chaîne Ibérique. *Trabajos sobre Neógeno-Cuaternario* (I.L.M., CSIC), **7**, 29-34.

Moissenet, E. (1983) Aspectos de la neotectónica en la fosa de Teruel. In: Comba, J.A. (ed.), *Geología de España, Libro Jubilar J.M. Ríos*, IGME, Madrid, vol. II: 427-446.

Moissenet, E. (1989) Les fosses néogenes de la Chaîne ibérique: leur evolution dans le temps. *Bull. Soc. Géol. France* (sér. 8), **5**, 919-926.

Mountney, N.P. (2006a) Eolian facies models. In: *Facies models revisited* (Eds. R.G. Walker and H. Posamentier) SEPM Mem., **84,** pp.19-83.

Mountney, N.P. (2006b) Periodic accumulation and destruction of aeolian erg sequences in the Permian Cedar Mesa Sandstone, White Canyon, southern Utah, USA. *Sedimentology*, **53**, 789-823.

Mountney, N.P. and **Howell, J.** (2000) Aeolian architecture, bedform climbing and preservation space in the Cretaceous Etjo Formation, NW Namibia. *Sedimentology*, **47**, 825-849.

Mountney, N.P. and **Thompson, D.B.** (2002) Stratigraphic evolution and preservation of aeolian dune and damp/wet interdune strata: an example from the Triassic Helsby Sandstone Formation, Cheshire Basin, UK. *Sedimentology*, **49**, 805-833.

Mosbrugger, V., Utescher, T. and **Dilcher, D.L.** (2005) Cenozoic continental climatic evolution of Central Europe. *PNAS*, **102**, 14964-14969.

Murat, A. (1999) Pliocene-Pleistocene occurrence of papropels in the western Mediterranean Sea and their relation to eastern Mediterranean sapropels. In: *Proceedings of the Ocean Drilling Program, Scientific Results, vol 161*, (Eds. R. Zahn, M.C. Comas, and A. Klaus). 519-527.

Nemec, W. and **Steel, R.J.** (1984) Alluvial and coastal conglomerates: their significant features and some comments on gravelly mass-flow deposits. In: *Sedimentology of Gravels and Conglomerates* (Eds. E.H. Koster & R.J. Steel). *Can. Soc. Petrol. Geol. Memoir*, **10**, 1-31.

Opdyke, N., Mein, P., Lindsay, E., Pérez-González, A., Moissenet, E. and **Norton, V.L.** (1997) Continental deposits, magnetostratigraphy and vertebrate paleontology, late Neogene of Eastern Spain. *Palaeogeography, Palaeoclimatology, Palaeoecology*, **133**, 129-148.

Janaway, T.M. and **Parnell, J.** (1989) Carbonate production within the orcadian basin, northern Scotland: A petrographic and geochemical study. *Palaeogeog., Palaeoclimatol., Palaeoecol.*, **70**, 89-105.

Ramos, A. and **Sopeña, A.** (1983) Gravel bars in low sinuosity streams (Permian and Triassic, Central Spain), In: *Modern and Ancient Fluvial Systems* (Eds. J. D. Collinson and J. Lewin). *IAS Spec. Publ.*, **6**, 301-312.

Ravelo, A.C., Andreasen, D.H., Lyle, M., Lyle, A.O. and **Wara, M.W.** (2004) Regional climate shifts caused by gradual global cooling in the Pliocene epoch. *Nature*, **429**, 263-267.

Rainbird, R.H., Hadlari, T., Aspler, L.B., Donaldson, J.A., Lecheminant, A.N. and **Peterson, D.T.** (2003) Sequence stratigraphy and evolution of the Paleoproterozoic intracontinental Baker Lake and Thelon basins, western Churchill Province, Nunavut, Canada. *Precambrian Research*, **125**, 21-53.

Roca, E. and **Guimerà, J.** (1992) The Neogene structure of the eastern Iberian margin: structural constraints on the crustal evolution of the Valencia trough (western Mediterranean). *Tectonophysics*, **203**, 203-218.

Rodríguez-López, J.P., Meléndez, N., de Boer, P.L. and **Soria, A.R.** (2008) Aeolian sand sea development along the Mid-Cretaceous Western Tethyan Margin (Spain): erg sedimentology and palaeoclimate implications. *Sedimentology*, **55**, 1253-1292.

Rodríguez-López, J.P., Meléndez, N., de Boer, P.L. and **Soria, A.R.** (2010) The action of wind and water in a back erg margin system close to the Variscan Iberian Massif. *Sedimentology*, **57**, 1315-1356.

Rodríguez-López, J.P., Meléndez, N., de Boer, P.L. and **Soria, A.R.** (2011) Controls on marine-erg margin cycle variability: aeolian-marine interaction in the mid-Cretaceous Iberian Desert System. Spain. *Sedimentology*, (in press) ***doi: 10.1111/j.1365-3091.2011.01261.x***

Rohling, E.J. and **Hilgen, F.J.** (1991) The eastern Mediterranean climate at times of sapropel formation: a review. *Geol. en Mijn.*, **70,** 253-264,

Rossignol-Strick, M. (1983) African monsoons, an immediate climatic response to orbital insolation, *Nature*, **303**, 46–49.

Roveri, M. and **Taviani, M.** (2003) Calcarenite and sapropel deposition in the Mediterranean Pliocene: shallow- and deep-water record of astronomically driven climatic events. *Terra Nova*, **15**, 279-286.

Rubio, J.C. and **Simón, J.L.** (2007) Tectonic subsidence vs. erosional lowering in a controversial intramontane depression: the Jiloca basin (Iberian Chain, Spain). *Geol. Mag*., **144(1)**, 1-15.

Saqqa, W. and **Atallah, M.** (2004) Characterization of the aeolian terrain facies in Wadi Araba Desert, southwestern Jordan. *Geomorphology*, **62**, 63-87.

Scherer, C.M.S. (2000) Eolian dunes of the Botucatu Formation (Cretaceous) in southernmost Brazil: morphology and origin. *Sed. Geol.*, **137**, 63-84.

Scherer, C.M.S., Lavina, E.L.C., Dias Filho, D.C., Oliveira, F.M., Bongiolo, D.E. and **Aguiar, E.S.** (2007) Stratigraphy and facies architecture of the fluvial-aeolian-lacustrine Sergi Formation (Upper Jurassic) Recôncavo Basin, Brazil. *Sed. Geol.,* **194**, 169-193.

Sierro, F.J., Ledesma, S., Flores, J.-A., Torrescusa, S. and del Olmo, W.M. (2000) Sonic and gamma-ray astrochronology: Cycle to cycle calibration of Atlantic climatic records to Mediterranean sapropels and astronomical oscillations. *Geology*, 28, 695-698.

Simón, J.L. (1982) *Compresión y distensión alpinas en la Cadena Ibérica Oriental*. Ph. D. Thesis, Universidad de Zaragoza. Publ. Instituto de Estudios Turolenses, Teruel (1984), 269 pp.

Simón, J.L. (1983) Tectónica y neotectónica del sistema de fosas de Teruel. *Teruel*, **69**, 21-97.

Simón, J.L. and **Paricio, J.** (1988) Sobre la compresión neógena en la Cordillera Ibérica. *Estudios Geológicos*, **44**, 271-283.

Sohn, Y.K. (2000) Coarse-grained debris-flow deposits in the Miocene fan deltas, SE Korea: a scaling analysis. *Sed. Geol.*, **130**, 45-64.

Sohn, Y.K., Choe, M.Y. and **Jo, H.R.** (2002) Transition from debris flow to hyperconcentrated flow in a submarine channel (the Cretaceous Cerro Toro Formation, southern Chile). *Terra Nova*, **14**, 405-415.

Soria, A.R., Liesa, C.L., Rodríguez-López, J.P., Meléndez, N., de Boer, P.L. and **Meléndez, A.** (2011) An Early Triassic evolving erg system (Iberian Chain, NE Spain): palaeoclimate implications. *Terra Nova*, **23**, 76-84.

Suc, J.-P., Diniz, F., Leroy, S., Poumot, C., Bertini, A., Dupont, L., Clet, M., Bessais, E., Zheng, Z., Fauquette, S., and Ferrier, J.: Zanclean (_Brunssumian) to early Piacenzian (_earlymidlle Reuverian) climate from 4_ to 54_ north latitude (West Africa, West Europe and West Mediterranean areas), Meded. Rijks Geol. Dienst, 52, 43–56, 1995.

Stanistreet, I.G. and **Stollhofen, H.** (2002) Hoanib River flood deposits of Namib Desert interdunes as analogues for thin permeability barrier mudstone layers in aeolianite reservoirs. *Sedimentology*, **49**, 719-736.

Svendsen, J., Stollhofen, H., Krapf, C.B.E., and **Stanistreet, I.G.** (2003) Mass and hyperconcentrated flow deposits record dune damming and catastrophic breakthrough of ephemeral rivers, Skelton Coast Erg, Namibia. *Sed. Geol.*, **160**, 7-31.

Turner, P. (1980) Continental red beds. *Developments in Sedimentology*, **29**, Elsevier, Oxford. 562 p.

Tzedakis, P.C. (2007) Seven ambiguities in the Mediterranean palaeoenvironmental narrative. *Quaternary Science Reviews*, **26,** 2042-2066.

van Dam, J.A. (1997) The small mammals from the upper Miocene of the Teruel-Alfambra region (Spain): Paleobiology and paleoclimatic reconstructions. Ph. D. Thesis, University of Utrecht, 204 pp.

van Dam, J.A. (2006) Geographic and temporal patterns in the late Neogene (12-3 Ma) aridification of Europe: The use of small mammals as paleoprecipitation proxies. *Palaeogeography, Palaeoclimatology, Palaeoecology*, **238**, 190-218.

van Dam, J.A., Alcalá, L., Alonso-Zaraza, A., Calvo, J.P., Garcés, M., and **Krijgsman, W.** (2001) The upper Miocene mammal record from the Teruel-Alfambra region (Spain). The MN system and continental stage/age concepts discussed. *Journal of Vertebrate Paleontology*, **21**, 367-385.

van Dam, J.A., Abdul Aziz, H., Álvarez Sierra, M.A., Hilgen, F.J., Hoek Ostende, L.W. van den, Lourens, L.J., Mein, P., Meulen, A.J. van der, and **Pelaez-Campomanes, P.** (2006) Long-period astronomical forcing of mammal turnover. *Nature*, **443**, 687-691.

Vegas, R., Fontboté, J.M., and **Banda, E.** (1979) Widespread Neogene rifting superimposed on alpine regions of the Iberian Peninsula. *Proceedings Symposium Evolution and Tectonics of the Western Mediterranean and Surrounding Areas*, EGS, Viena. Instituto Geográfico Nacional, Madrid, Special Publication 201, 109-128.

Wehausen, R. and **Brumsack, H.J.** (1998) The formation of Pliocene Mediterranean sapropels: constraints from high-resolution major and minor element studies. *Proc. ODP Sci. Res*., **160**, 207–218.

Weerd, A. van de (1976) Rodent faunas of the Mio-Pliocene continental sediments of the Teruel-Alfambra region, Spain. *Utrecht Micropaleontol. Bulletin*, Special Publication 2, 217 pp.

Wilkins, D.E. and **Ford, R.L.** (2007) Nearest neighbor methods applied to dune field organization: The Coral Pink Sand Dunes, Kane County, Utah, USA. *Geomorphology*, **83**, 48-57.

Van Zinderen Bakker, E.M. and Mercer, J.H. (1986) Major late Cainozoic climatic events and palaeoenvironmental changes in Africa viewed in a world wide context. *Palaeogeography, Palaeoclimatology, Palaeoecology*, **56,** 217-235.

TABLE AND FIGURE CAPTIONS

Table 1. Wind-related and water-related facies associations.

Figure 1. The study area. (A) The NNE–SSW trending Teruel Basin in the central-eastern Iberian Chain (NE Spain). Note the perpendicular orientation relative to the main NW–SE structural trend of the Iberian Chain. (B) Geological map of the northern part of the Teruel Basin with the location of the study area (modified after Rubio & Simón (2007). (C) Simplified geological cross-section [see (B) for location] showing the half-graben structure of the basin in the Escorihuela sector. (D) Scheme (with tentative scale) with the Neogene–Quaternary lithological units cropping out near Escorihuela [see location in (C)]: Peral Formation (Vallesian, Late Miocene), Alfambra Formation. (Late Miocene–Early Pliocene), Escorihuela Formation (Middle–Late Pliocene) with the aeolian-fluvial deposits (Es), and Late Pliocene–Quaternary (Pleistocene) pediment (glacis) deposits (Gl). (C) and (D) modified after Lafuente *et al.* (2008). (E) Photograph of the Sierra del Pobo Fault and the Teruel half-graben deposits. (F) Location of the five stratigraphic sections.

Figure 2. (A) Correlation of the Escorihuela section (present study) with previous logs. GPTS correlation of Opdyke et al. (1997) reinterpreted by Oms et al. (1999). (B) and (C) The Late Pliocene aeolian yellow sands in the Escorihuela Quarry (section E-3; location in Fig. 1). Photograph shows from base to top: aeolian deposits, wind-water interaction deposits and the uppermost pediment (glacis) gravel. (D) Rose diagram and stereographic projection (lower hemisphere) of all measured metric-scale cross-stratification planes, and 1% density diagram of poles (5% contour interval) indicating the mean palaeowind direction towards the east (red arrow).

Figure 3. (A) Photograph and (B) line-drawing of large-scale and laterally continuous cross-bedded aeolian dune sandstones 100 m south of section E-4. Aeolian dune foresets display reactivation surfaces 'R' and are sharply covered by water-laid deposits. (C) Close-up of (B) [see location in (B)] showing the erosional relief on top of the dune foreset and the lateral intertonguing between the aeolian due toeset and the damp interdune deposits.

Figure 4. (A) Large-scale cross-bedded aeolian dune sandstones at section E-3 showing superimposition 'S' surfaces (B) and reactivation 'R' surfaces (C). (D) and (E) Aeolian dune toeset with interbedded grain flow 'gf' and wind ripple 'wr' lamination. Note the coarser grain flow deposits 'gf' and finer-grained laminated wind ripple deposits 'wr'.

Figure 5. (A) Aeolian sandsheet deposits with laterally continuous lamination penetrated by calcified roots. (B) Close up of aeolian sandsheet deposits showing, from base to top, bimodal aeolian deposits, an armoured surface and inversely graded wind ripple lamination. (C) Subcritically climbing translatent strata formed by migrating wind ripples in the aeolian sandsheet surface. Note the pin-stripe lamination. (D) Granule ripple with internal cross-lamination. (E) Adhesion ripple lamination. Images from sections E-3 (A) to (C) and E-5 (D) and (E).

Figure 6. (A) Low-angle aeolian deposits. (B) Close up of (A) showing laterally continuous granule lag. (C) Close up of (B); note that granules are aligned and lie isolated along the lineation. (D) Well-sorted and rounded granules forming an armoured pavement due to (long-lasting) deflation of the low-angle aeolian deposits.

Figure 7. (A) Photograph and (B) line-drawing of a channel, deeply encased in aeolian sandsheet sandstones, and filled with intraformational conglomerate (section E-5). The channel fill mainly consists of reworked aeolian sand blocks covered by extraformational conglomerates and aeolian sandsheet sands. (C) and (D) close up of (A) showing the sharp contact of the channel base eroding the underlying aeolian sandsheet lamination. Note the well-preserved lamination within the aeolian sand blocks. (E) Erosional truncation of the aeolian sandsheet by the high-angle channel margin. (F) V-shaped channel base covered by well-preserved angular aeolian sandstone blocks.

Figure 8. (A) Debris flow conglomerates characterized by a sharp-flat base with inverse grading, interbedded with sandy tabular sediments deposited by waning traction current after debris flow emplacement. (B) Crudely bedded cobble-sand sheetflood with slightly erosional bases and interbedded aeolian sandstones. (C) Vertically stacked channellized boulder-sand bedload stream deposits interbedded with aeolian sandstones. (D) Stream deposits with large-scale cross-bedding and a deep incision into the underlying fine-grained deposits. (E) Multi-storey boulder-sand bedload stream deposits showing lagged gravel pockets with local carbonate blocks. Images from the upper part of section E-3 (A), (D), and (E) and section E-5 (B) and (C).

Figure 9. (A) Pebbly-sand bedload stream deposits encased in aeolian sandstones in the uppermost part of section E-4. (B), (C) and (D) are close-ups of (A). (B) Basal erosive surface and gravel lag over aeolian sandstones. (C) Vertical wall of channel base cutting aeolian pin-stripe lamination. (D) Sharp contact between the upper coarser stream sandstones and the pin-

stripe lamination of the underlying aeolian sandstones. (E) Lacustrine carbonates with intense rooting covering aeolian sandstones at section E-2.

Figure 10. Animal tracks in aeolian deposits at section E-3. (A) Several layers affected by animal tracks separated by non-deformed and laminated deposits. (B) Track showing folded lamination, vertical walls, two marginal upfolds and lateral diminution of thickness from non-deformed zones to folded zones. (C) Bilobate track with marginal upfolds. (D) Track characterized by vertical walls. The track was filled by successive grain flows, and is covered by adhesion ripple cross-lamination. (E) Track showing laminated infill. (F) Partly carbonate-cemented animal track. Note partial brecciation of pin-stripe lamination.

Figure 11. (A) Deformed level and scattered tracks at section E-3. (B) Close-up of the upper part of (A) showing three layers affected by animal tracks, separated by non-deformed lamination. (C) Close-up of the middle part of (A) showing a strongly disrupted level formed by at least two track intervals. Brecciation of lamination is observed in the lower-right corner. Local fill of V-shaped tracks by grain flows (upper part).

Figure 12. (A) Correlation panel showing the different facies associations and their lateral relations. (B) Location of the studied area close to the Sierra del Pobo Fault. (C) Location of the studied stratigraphic sections E1 to E5. (D) Photograph showing the location of sections E1 to E3 and their location relative to the Sierra del Pobo Fault.

Figure 13. (A) Cartoon of the Pliocene depositional system during arid stages showing migration of the aeolian dune field toward the El Pobo Range, and encroachment of the alluvial fan toes. The Sierra del Pobo Fault controlled the accumulation and preservation of aeolian deposits. See legend in Fig. 14. (B) and (C) Aeolian deposits developed during these stages.

Figure 14. (A) Cartoon of the Pliocene depositional system during more humid stages leading to destruction and reworking of the aeolian dune field and recharge of distal carbonate ponds. (B) During these stages animal tracks in aeolian deposits were preserved. (C) A higher phreatic level favoured plant colonization leading to intense rootling. (D) Torrential and flashy discharge transported carbonate clasts from the adjacent relief. (E) Carbonate ponds recharged by ground water flow.

Figure 15. Satellite imagery from Google Earth (2010) of recent aeolian sand seas. (A) and (B) aeolian dune fields and alluvial fans in the Wadi Arava depression (Arava Valley, Death Sea Transform Valley) bounded by the Arava Fault. (C) and (D) The Coral Pink Sand Dunes in Utah, where the Sevier fault escarpment bounds part of the aeolian dune field. (E) The Lençóis Maranhenses National Park aeolian dunes (Brazil) showing straight boundaries that coincide with drainage paralleling the Pirapemas lineament. (F) Vegetation developed in ephemeral channels and aeolian dune aprons in the Namib Desert. (G) Partial destruction of an aeolian dune field by water flows in southern Pakistan.

Figure 16. Correlation of continental Iberian and marine Mediterranean deposits. (A) Magnetic polarity pattern Escorihuela section, Spain (Opdyke et al., 1997; Oms et al., 1999) and correlation to numerical time scale (Lourens et al., 2004). (B) Escorihuela section (this study). (C) Escorihuela parallel section (Opdyke et al. 1997). (D) Reconstructed coldest month temperature and precipitation in NE Spain based on Garraf pollen core offshore Barcelona (Fauquette et al. 1998); mean annual precipitation (MAP) and average minimum temperature (MINT). (E) Sonic log At3 Gulf of Cadiz; record and correlation to (F) after Sierro et al. (2000). (F) Northern Hemisphere 65º N summer insolation (after Laskar et al., 2004). Arrows indicate precession-controlled insolation maxima, whose alternation in strength reflects obliquity. (G) Sapropel-marl alternation Rossello (Sicily) and correlation to (F) (based on Hilgen, 1991). (H) Magnetic polarity pattern Rossello and correlation to Geomagnetic Polarity Time Scale (Hilgen, 1991).

Table 1. Facies Associations

FACIES ASSOCIATION	LITHOLOGY & GEOMETRY	SEDIMENTARY STRUCTURES	REFERENCES
Aeolian dunes	Pale to yellow fine to coarse-grained sandstones. Tabular, laterally continuous bodies	Large-scale trough cross-bedded sets; aeolian bounding surfaces (reactivation, superimposition surfaces). Grainflow deposits and wind ripple lamination	Kocurek, 1996; Mountney, 2006a,b; Scherer, 2000
Aeolian sandsheets	Flat-horizontal, tabular bodies formed by fine-grained yellowish sandstone organized in tabular metre-thick intervals	Subcritically climbing translatent strata, granule ripples, adhesion ripples, granule pavements, pin-stripe lamination. Root traces	Hunter, 1977; Fryberger *et al*. 1983; Clemmensen & Abrahamsen, 1983; Kocurek & Fielder, 1982
Low angle aeolian deposits	Laterally extensive sand bodies, layers dipping ≤15°. Fine to coarse-grained sandstones and granules	Subcritically climbing translatent strata, wind ripples. Interbedded dipping fine-grained and coarse-grained to granule layers. Granule pavements, granule linings	Fryberger *et al*., 1992; Kocurek, 1986; Maxwell & Hayness, 2001; Clemmensen & Abrahamsen, 1983
Intraformational conglomerate channel fill	Sub-rounded to sub-angular finely laminated sandstone blocks forming disorganized conglomerates infilling ribbon-like channelled bases. Sandy matrix and floating extraformational pebbles	No specific orientation of sandstone blocks	Deynoux *et al*., 1989; Mountney & Howell, 2000.
Debris flow	Tabular intervals of pebble-boulder, clast to matrix-supported disorganized to poorly organized conglomerates. Sharp-flat to slightly erosive bases. Sandy tabular intervals with floating pebbles and cobbles	Generally massive and disorganized; locally crude lamination; inverse rading; large protruding boulders at the top. Locally crudely imbricated clasts and parallel alignment of clasts. Vertically oriented clasts	Chamyal *et al*., 1997; Nemec & Steel, 1984; Sohn, 2000; Enos, 1977
Cobble-sand sheetfloods	Tabular and laterally continuous intervals. Conglomerates with slightly erosive bases	Internal crude cross-bedding	Turner, 1980.
Boulder to sand bedload streams	Metre-thick lenticular clast-supported channellized conglomerates. Massive conglomerates infilling ribbon-like channels with overhanging walls. Matrix of pebbly sand. Superimposed concave-up surfaces	Medium-scale cross-bedding. Foresets dip near 23°. Large-scale planar cross-bedding sets with dips near 11°	Chamyal *et al*., 1997; Ramos & Sopeña, 1983; Jo *et al*., 1997; Bhiry & Occhietti, 2004
Pebbly-sand bedload stream deposits	Fine to medium-grained sandstones with basal cobble lags. Lower sharp and erosive bases with vertical walls. Gravel pockets	Crude horizontal lamination, planar to tangential cross-bedded sets.	Blair, 1999; Jo *et al*., 1997
Sand-silt sheetfloods	Tabular metre to decimetre-thick intervals of muddy sandstones and siltstones	Structureless, mottling	Collinson, 1996; Jo *et al*., 1997
Damp interdunes	Tabular metre-thick intervals. Sandy mudstones and siltstones. Merging laterally with aeolian dune toesets	Laterally continuous lamination	Mountney & Thompson, 2002; Stanistreet & Stolhofen, 2002
Carbonate ponds	White micritic metre-thick carbonate intervals. Gastropods	Intensively rooted	Sanz et al., 1995

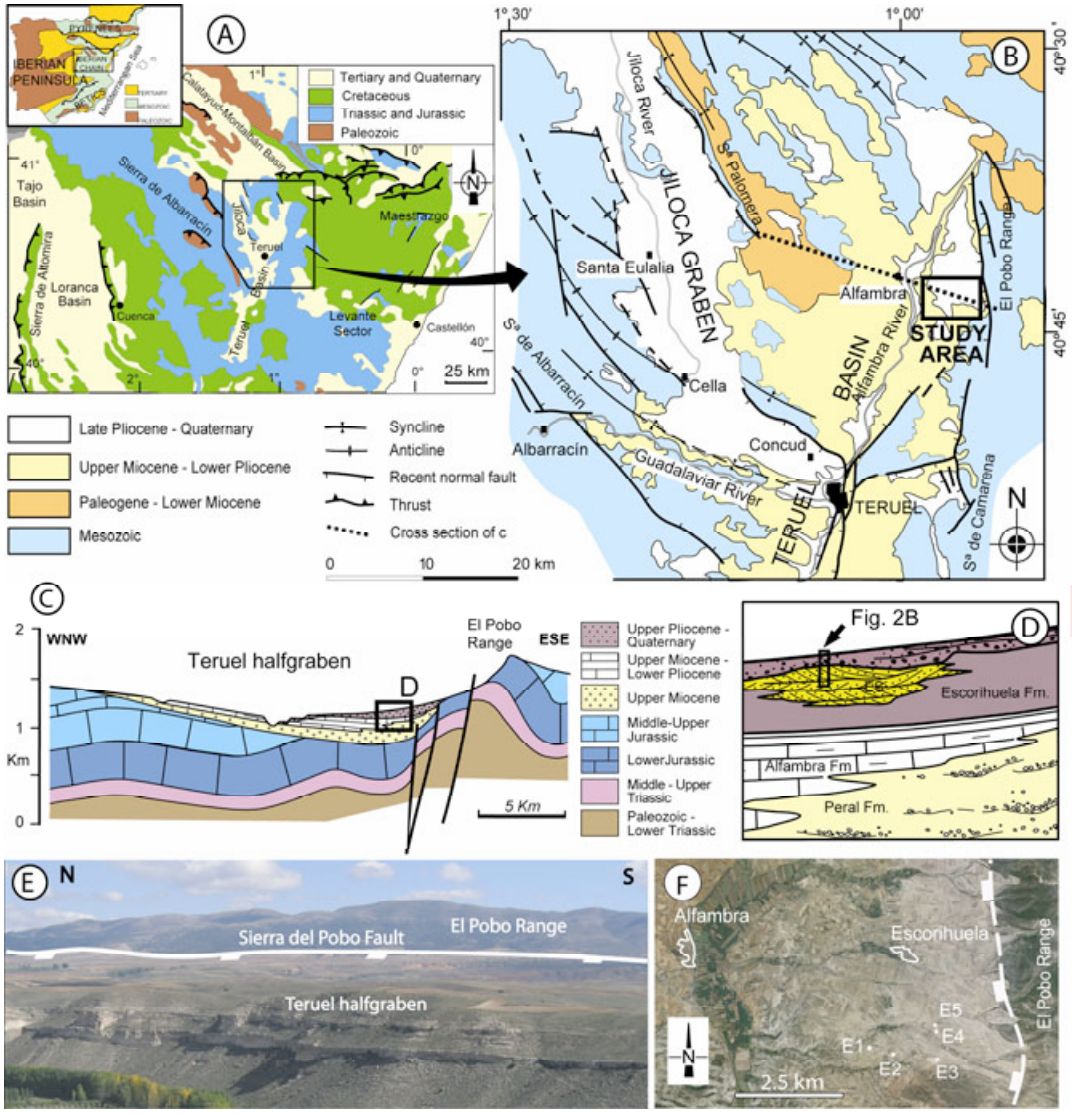
A
IBERIAN PENINSULA
Tertiary and Quaternary
Cretaceous
Triassic and Jurassic
Paleozoic
Tajo Basin
Sierra de Albarracín
Jiloca Basin
Teruel
Maestrazgo
Loranca Basin
Sierra de Altomira
Cuenca
Teruel Basin
Levante Sector
Castellón
25 km
B
1°30'
1°00'
40°30'
40°45'
Jiloca River
Sª Palomera
JILOCA GRABEN
Santa Eulalia
Alfambra
El Pobo Range
STUDY AREA
BASIN
Alfambra River
Sª de Albarracín
Cella
Albarracín
Concud
Guadalaviar River
TERUEL
Sª de Camarena
N
Late Pliocene - Quaternary
Upper Miocene - Lower Pliocene
Paleogene - Lower Miocene
Mesozoic
Syncline
Anticline
Recent normal fault
Thrust
Cross section of c
0 10 20 km
C
WNW
ESE
Teruel halfgraben
El Pobo Range
D
2
1
Km
0
5 Km
Upper Pliocene - Quaternary
Upper Miocene - Lower Pliocene
Upper Miocene
Middle-Upper Jurassic
LowerJurassic
Middle - Upper Triassic
Paleozoic - Lower Triassic
Fig. 2B
D
Escorihuela Fm.
Alfambra Fm.
Peral Fm.
E
N
S
Sierra del Pobo Fault
El Pobo Range
Teruel halfgraben
F
Alfambra
Escorihuela
El Pobo Range
E5
E4
E1
E2
E3
N
2.5 km

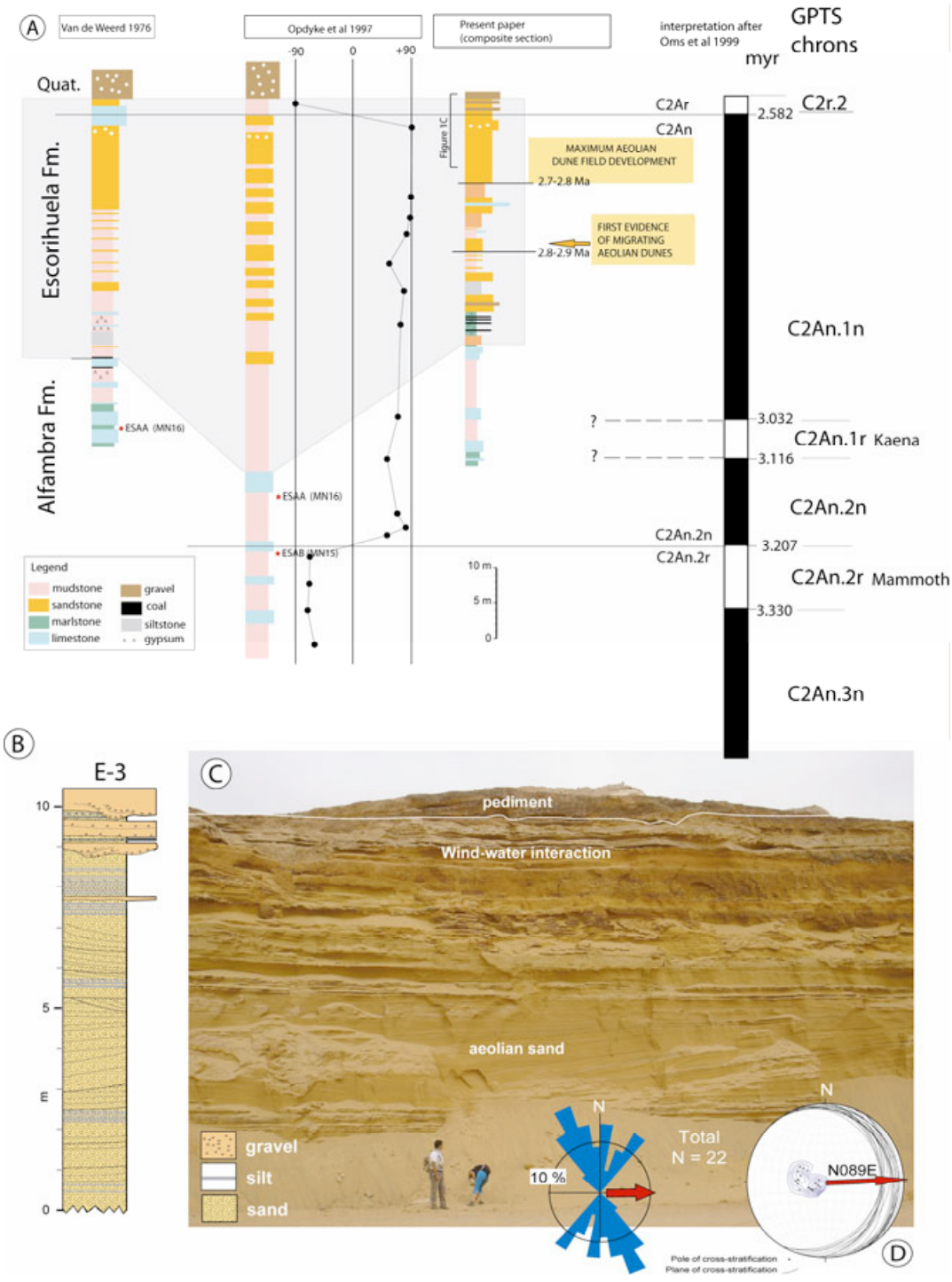
A
Van de Weerd 1976
Opdyke et al 1997
-90
0
+90
Present paper
(composite section)
interpretation after
Oms et al 1999
GPTS
chrons
myr
Quat.
Escorihuela Fm.
Alfambra Fm.
ESAA (MN16)
ESAA (MN16)
ESAB (MN15)
Figure 1C
C2Ar
C2An
2.582
C2r.2
MAXIMUM AEOLIAN
DUNE FIELD DEVELOPMENT
2.7-2.8 Ma
FIRST EVIDENCE
OF MIGRATING
AEOLIAN DUNES
2.8-2.9 Ma
C2An.1n
?
3.032
C2An.1r Kaena
?
3.116
C2An.2n
C2An.2n
C2An.2r
3.207
C2An.2r Mammoth
3.330
C2An.3n
Legend
mudstone
sandstone
marlstone
limestone
gravel
coal
siltstone
gypsum
10 m
5 m
0
B
E-3
10
5
m
0
C
pediment
Wind-water interaction
aeolian sand
gravel
silt
sand
N
10 %
Total
N = 22
N
N089E
D
Pole of cross-stratification
Plane of cross-stratification

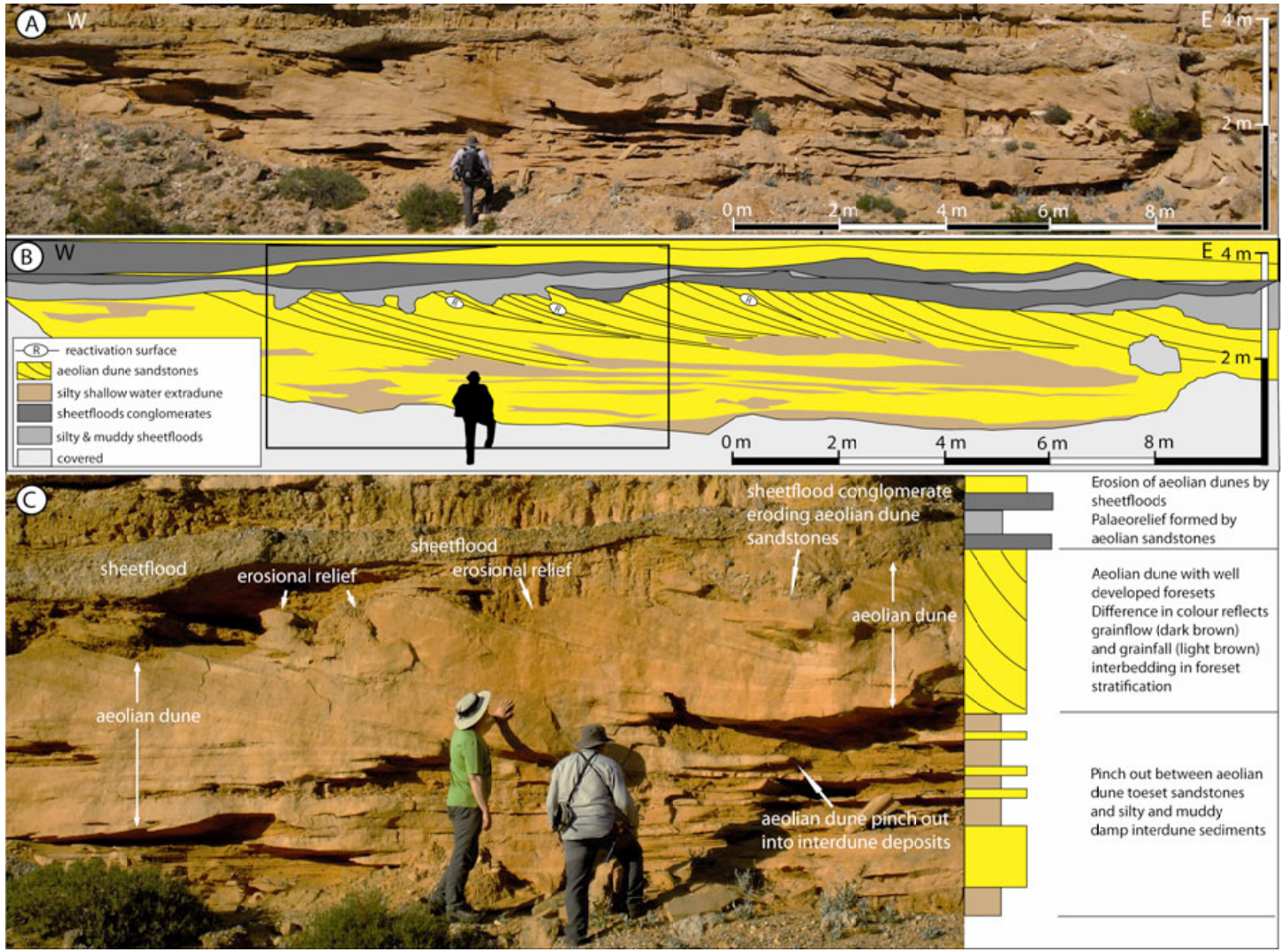
A
W
E
4 m
2 m
0 m
2 m
4 m
6 m
8 m
B
W
E
4 m
2 m
R
reactivation surface
aeolian dune sandstones
silty shallow water extradune
sheetfloods conglomerates
silty & muddy sheetfloods
covered
0 m
2 m
4 m
6 m
8 m
C
sheetflood
erosional relief
sheetflood
erosional relief
sheetflood conglomerate
eroding aeolian dune
sandstones
aeolian dune
aeolian dune
aeolian dune pinch out
into interdune deposits
Erosion of aeolian dunes by
sheetfloods
Palaeorelief formed by
aeolian sandstones
Aeolian dune with well
developed foresets
Difference in colour reflects
grainflow (dark brown)
and grainfall (light brown)
interbedding in foreset
stratification
Pinch out between aeolian
dune toeset sandstones
and silty and muddy
damp interdune sediments

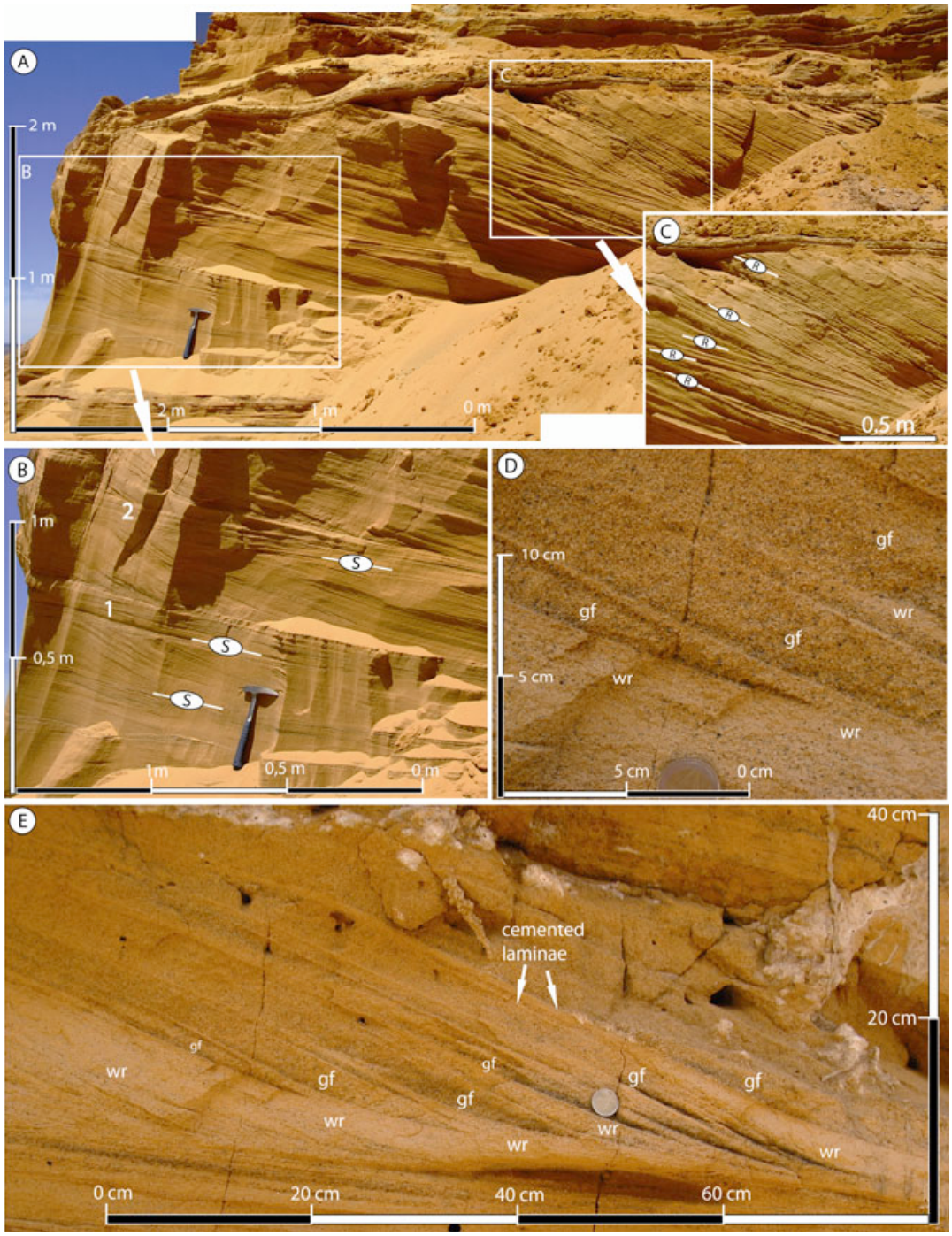
A
2 m
B
1 m
C
2 m
1 m
0 m
C
R
R
R
R
R
0.5 m
B
1m
2
1
S
S
S
0,5 m
1m
0,5 m
0 m
D
10 cm
5 cm
gf
gf
gf
wr
wr
wr
5 cm
0 cm
E
40 cm
20 cm
cemented
laminae
gf
wr
gf
gf
gf
gf
gf
wr
wr
wr
wr
0 cm
20 cm
40 cm
60 cm

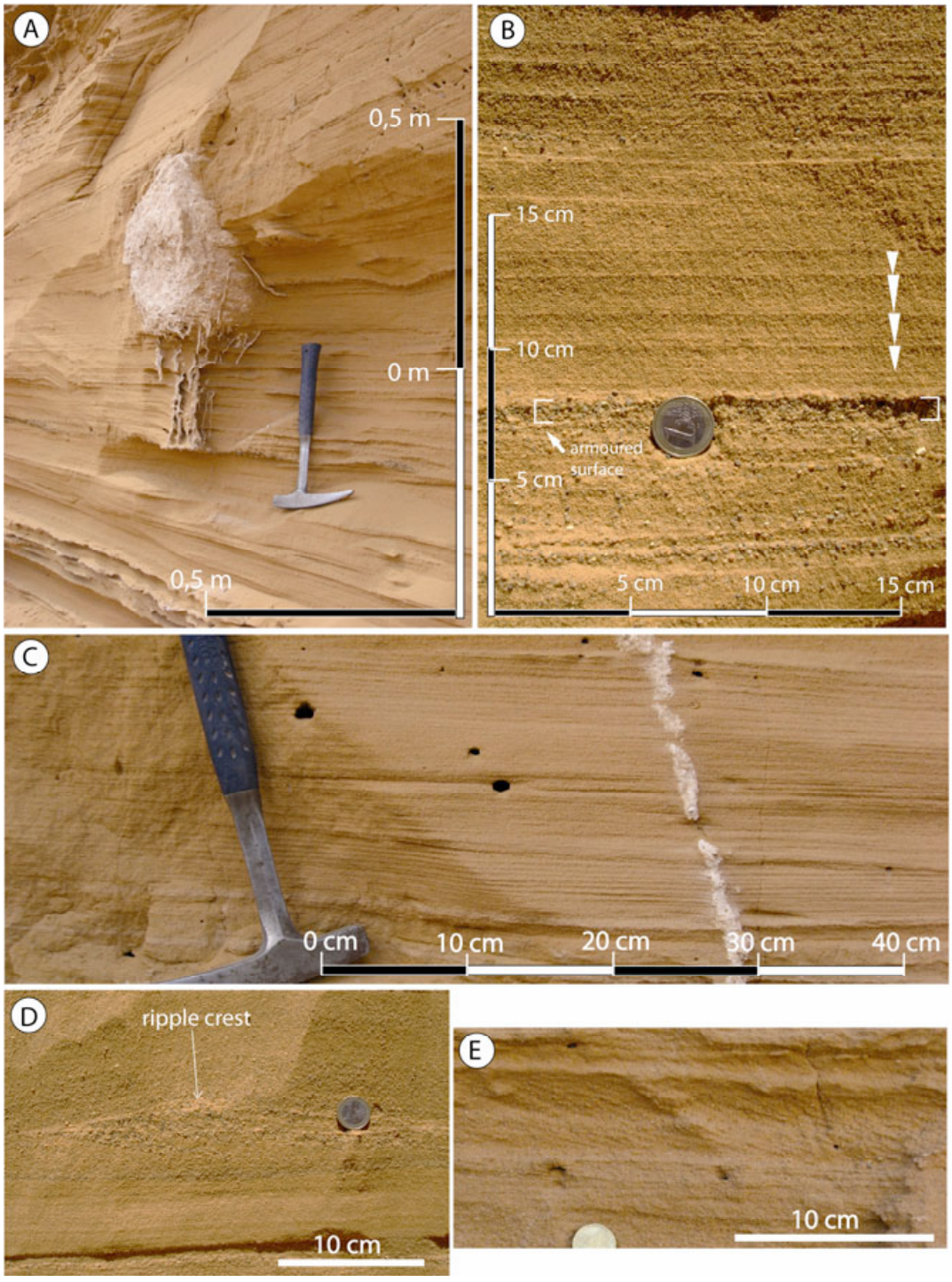
A
0,5 m
0 m
0,5 m
B
15 cm
10 cm
armoured
surface
5 cm
5 cm
10 cm
15 cm
C
0 cm
10 cm
20 cm
30 cm
40 cm
D
ripple crest
10 cm
E
10 cm

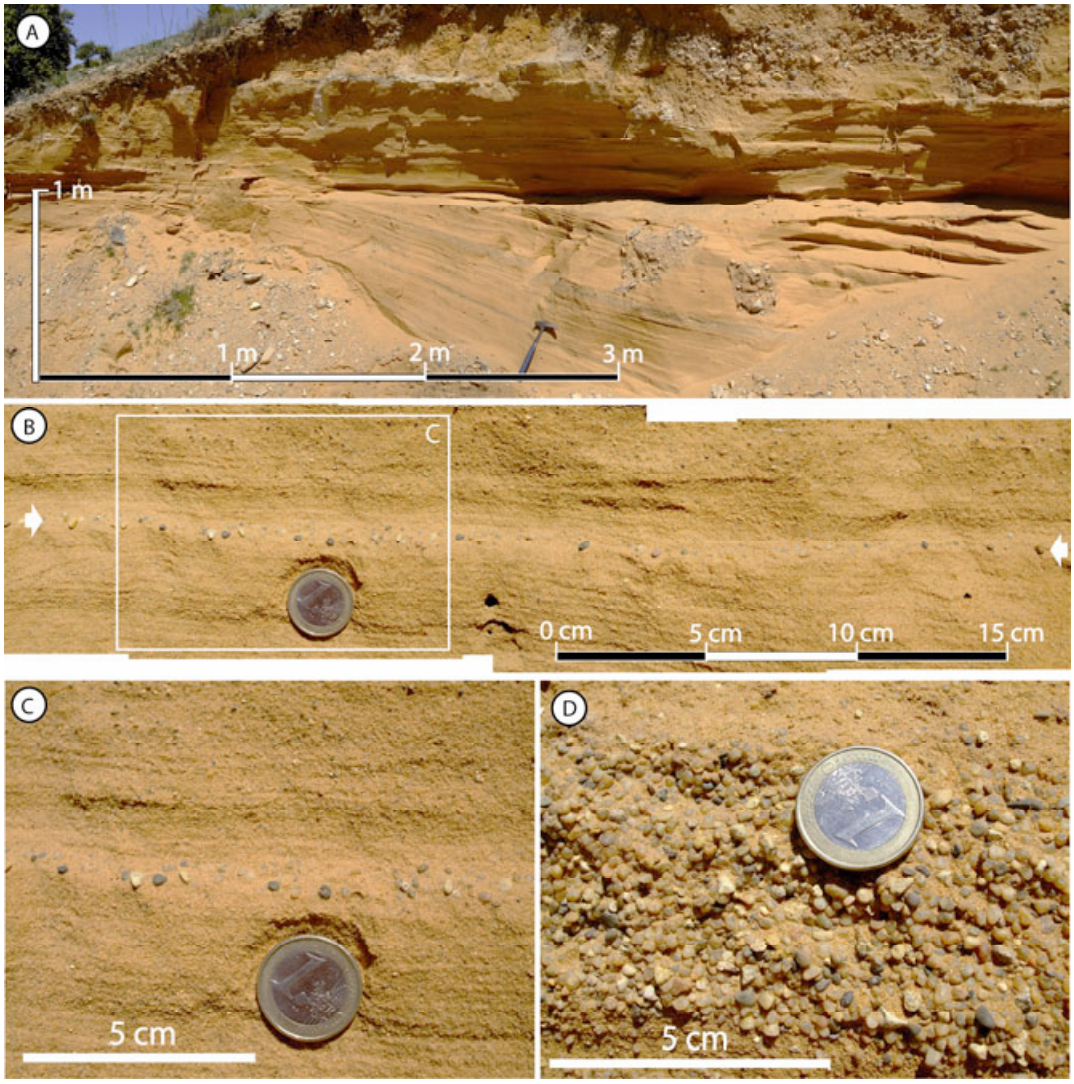
A
1 m
1 m
2 m
3 m
B
C
0 cm
5 cm
10 cm
15 cm
C
5 cm
D
5 cm

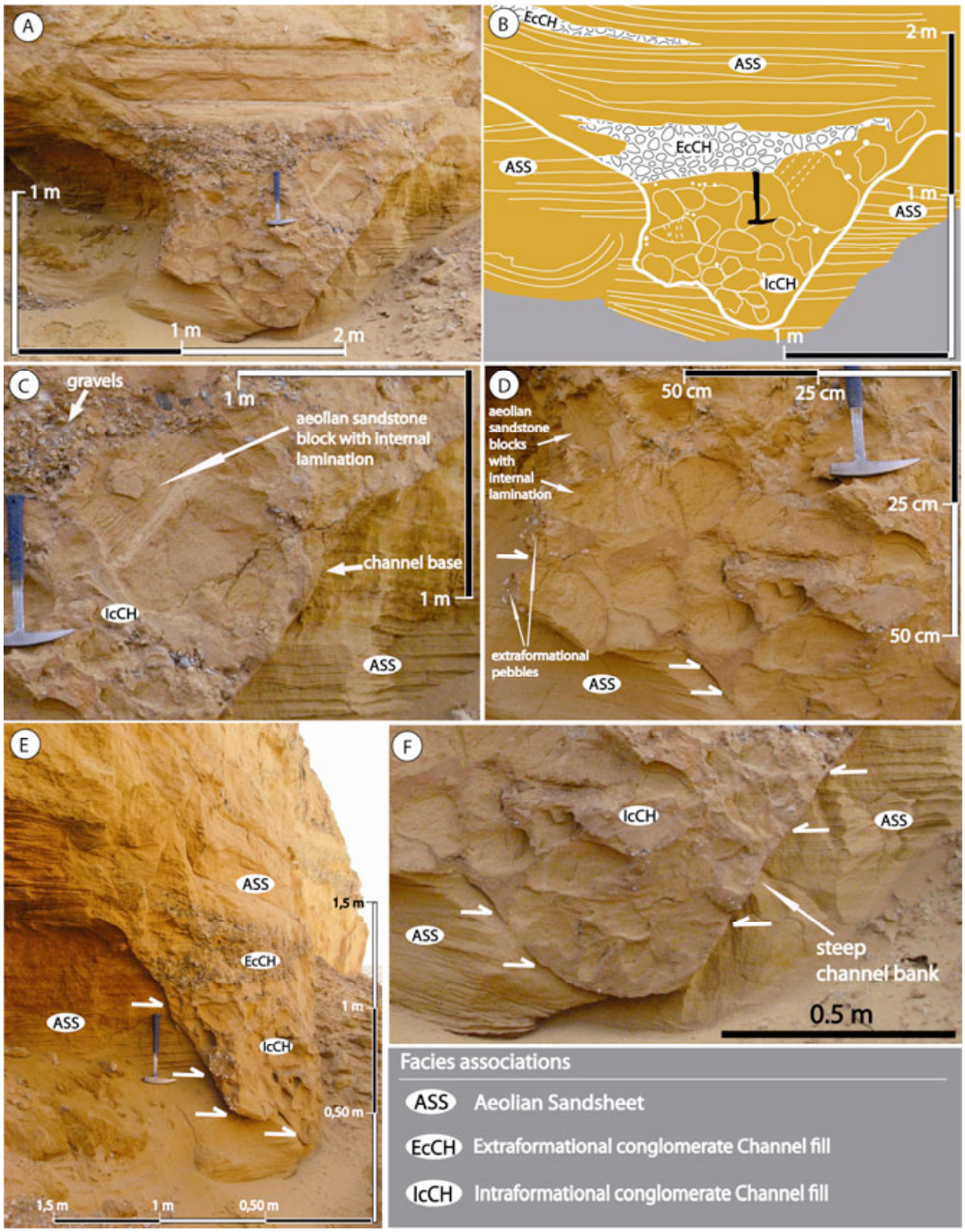
A
1 m
1 m
2 m
B
EcCH
2 m
ASS
EcCH
ASS
1 m
ASS
IcCH
1 m
C
gravels
1 m
aeolian sandstone block with internal lamination
channel base
1 m
IcCH
ASS
D
50 cm
25 cm
aeolian sandstone blocks with internal lamination
25 cm
50 cm
extraformational pebbles
ASS
E
ASS
1,5 m
EcCH
1 m
ASS
IcCH
0,50 m
1,5 m
1 m
0,50 m
F
IcCH
ASS
ASS
steep channel bank
0.5 m
Facies associations
ASS Aeolian Sandsheet
EcCH Extraformational conglomerate Channel fill
IcCH Intraformational conglomerate Channel fill

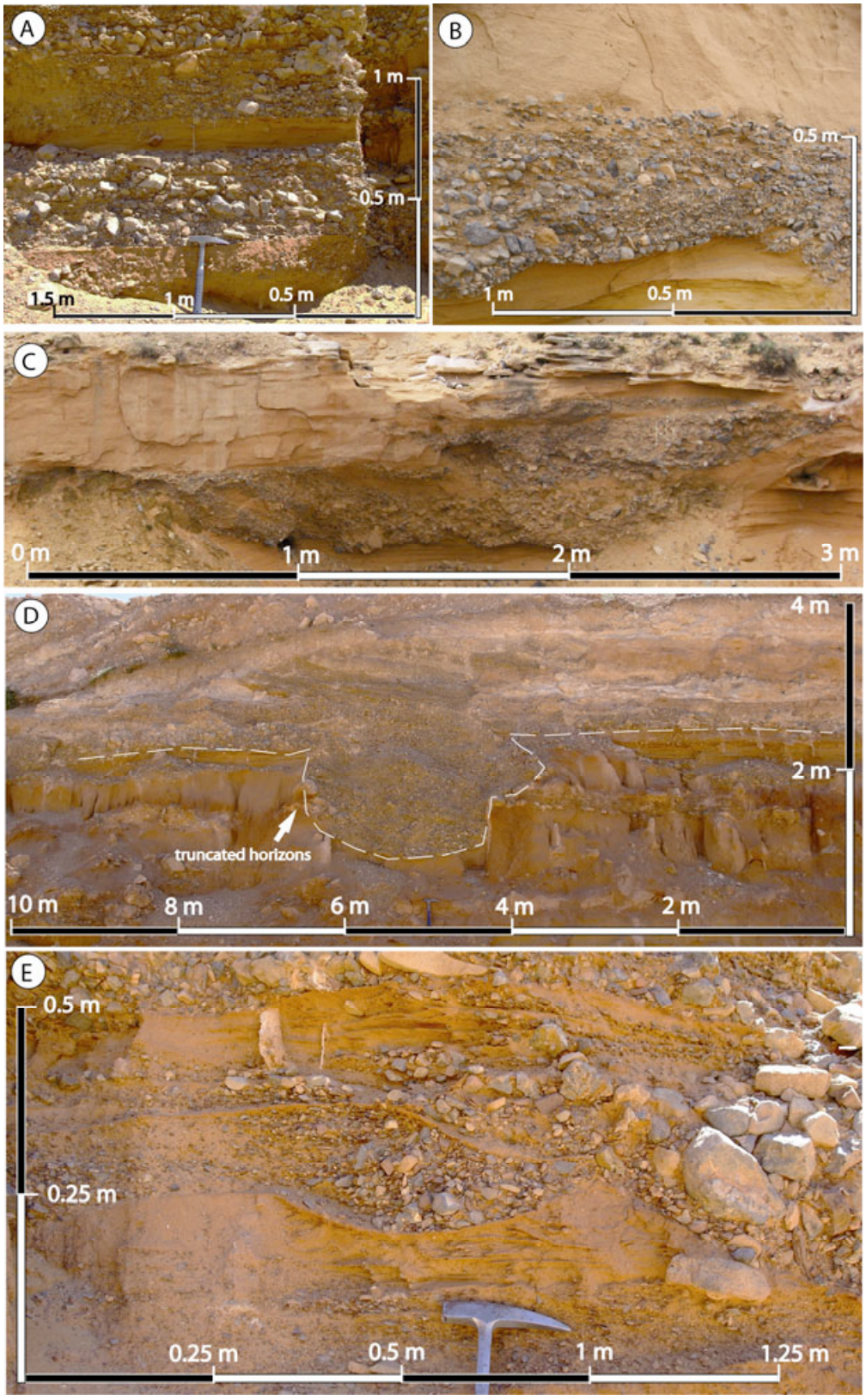
A
1 m
0.5 m
1.5 m
1 m
0.5 m
B
0.5 m
1 m
0.5 m
C
0 m
1 m
2 m
3 m
D
4 m
2 m
truncated horizons
10 m
8 m
6 m
4 m
2 m
E
0.5 m
0.25 m
0.25 m
0.5 m
1 m
1.25 m

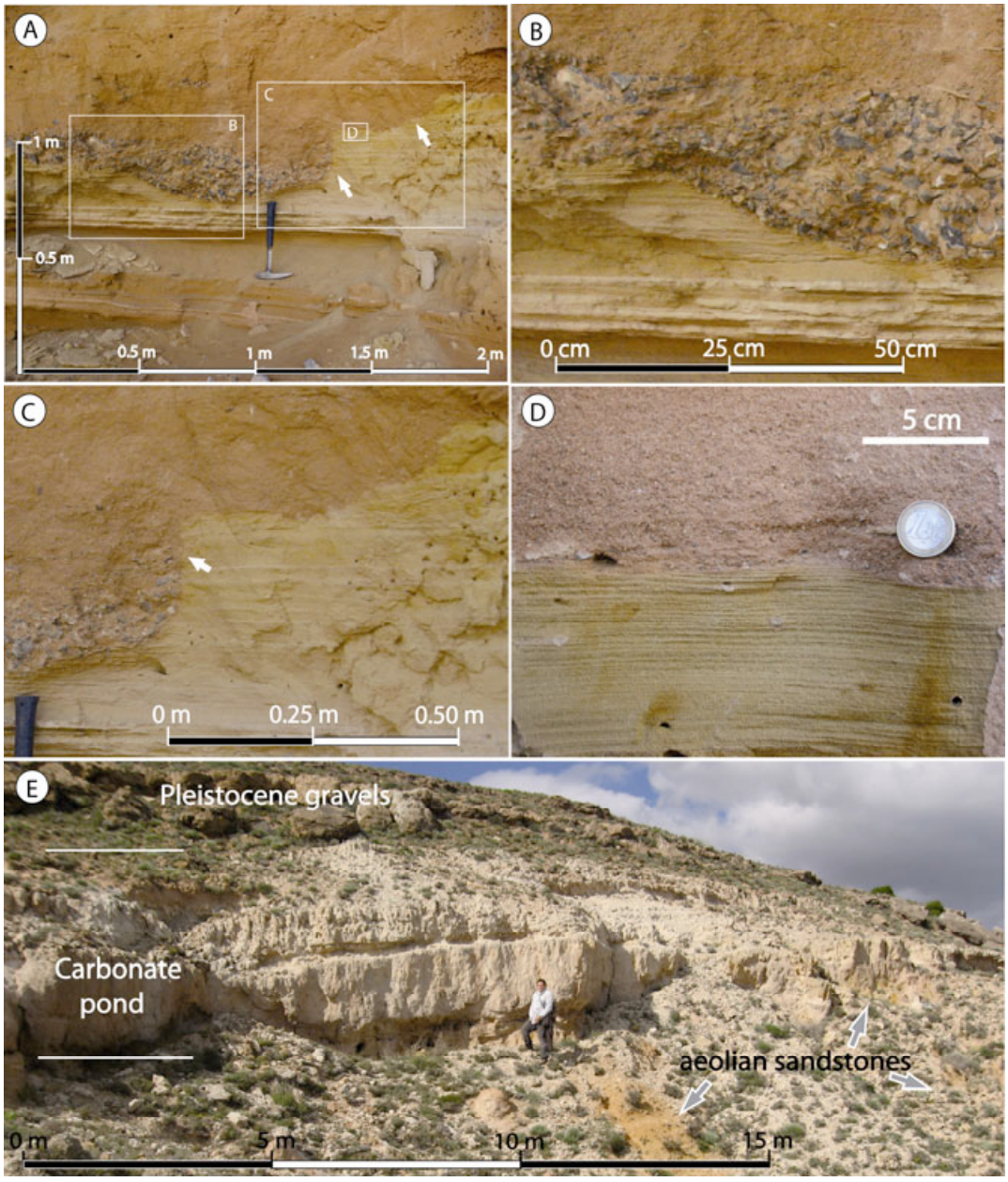
A
B
C
D
1 m
0.5 m
0.5 m
1 m
1.5 m
2 m
0 cm
25 cm
50 cm
0 m
0.25 m
0.50 m
5 cm
E
Pleistocene gravels
Carbonate
pond
aeolian sandstones
0 m
5 m
10 m
15 m

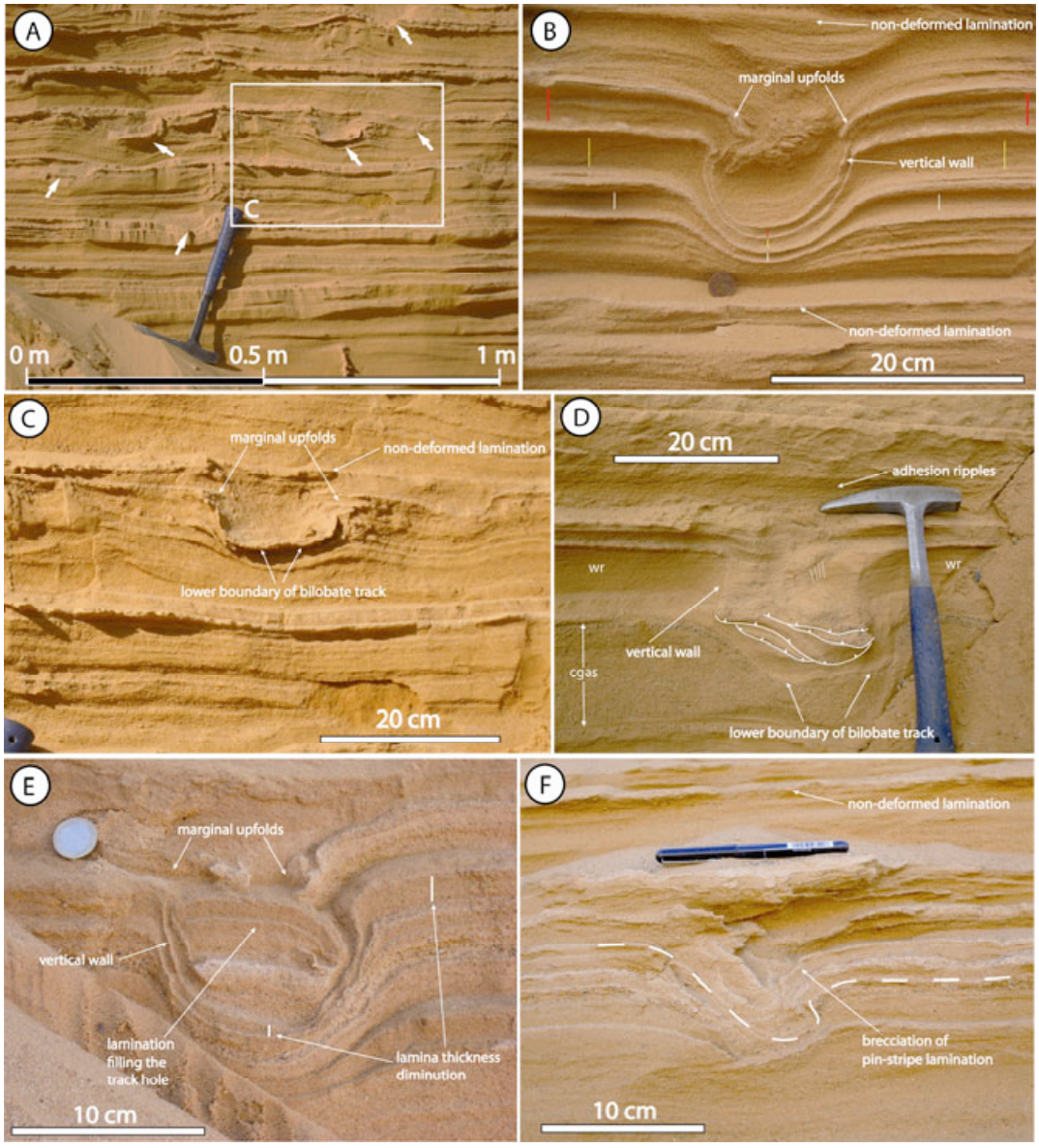
A
C
0 m
0.5 m
1 m
B
non-deformed lamination
marginal upfolds
vertical wall
non-deformed lamination
20 cm
C
marginal upfolds
non-deformed lamination
lower boundary of bilobate track
20 cm
D
20 cm
adhesion ripples
wr
wr
vertical wall
cgas
lower boundary of bilobate track
E
marginal upfolds
vertical wall
lamination filling the track hole
lamina thickness diminution
10 cm
F
non-deformed lamination
brecciation of pin-stripe lamination
10 cm

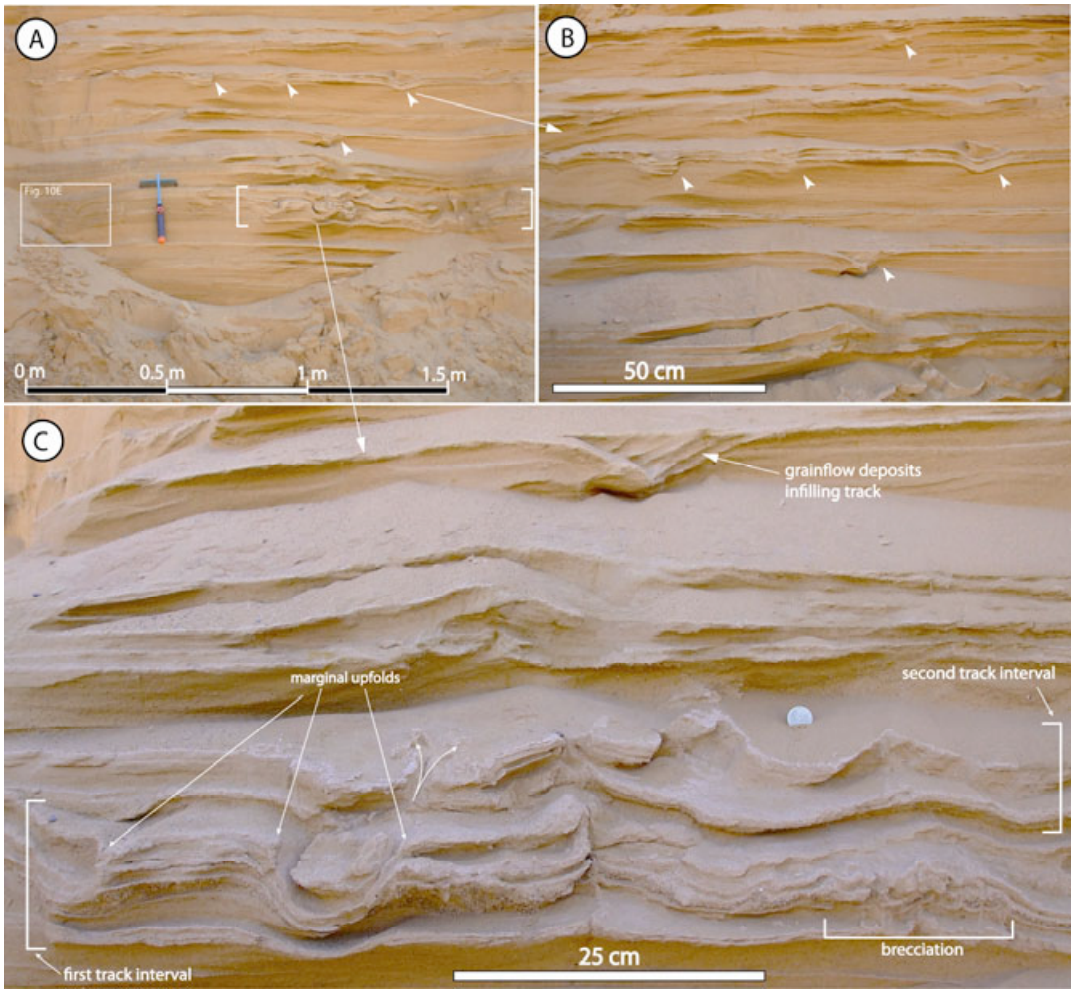
A
Fig. 10E
0 m
0.5 m
1 m
1.5 m
B
50 cm
C
grainflow deposits
infilling track
marginal upfolds
second track interval
brecciation
first track interval
25 cm

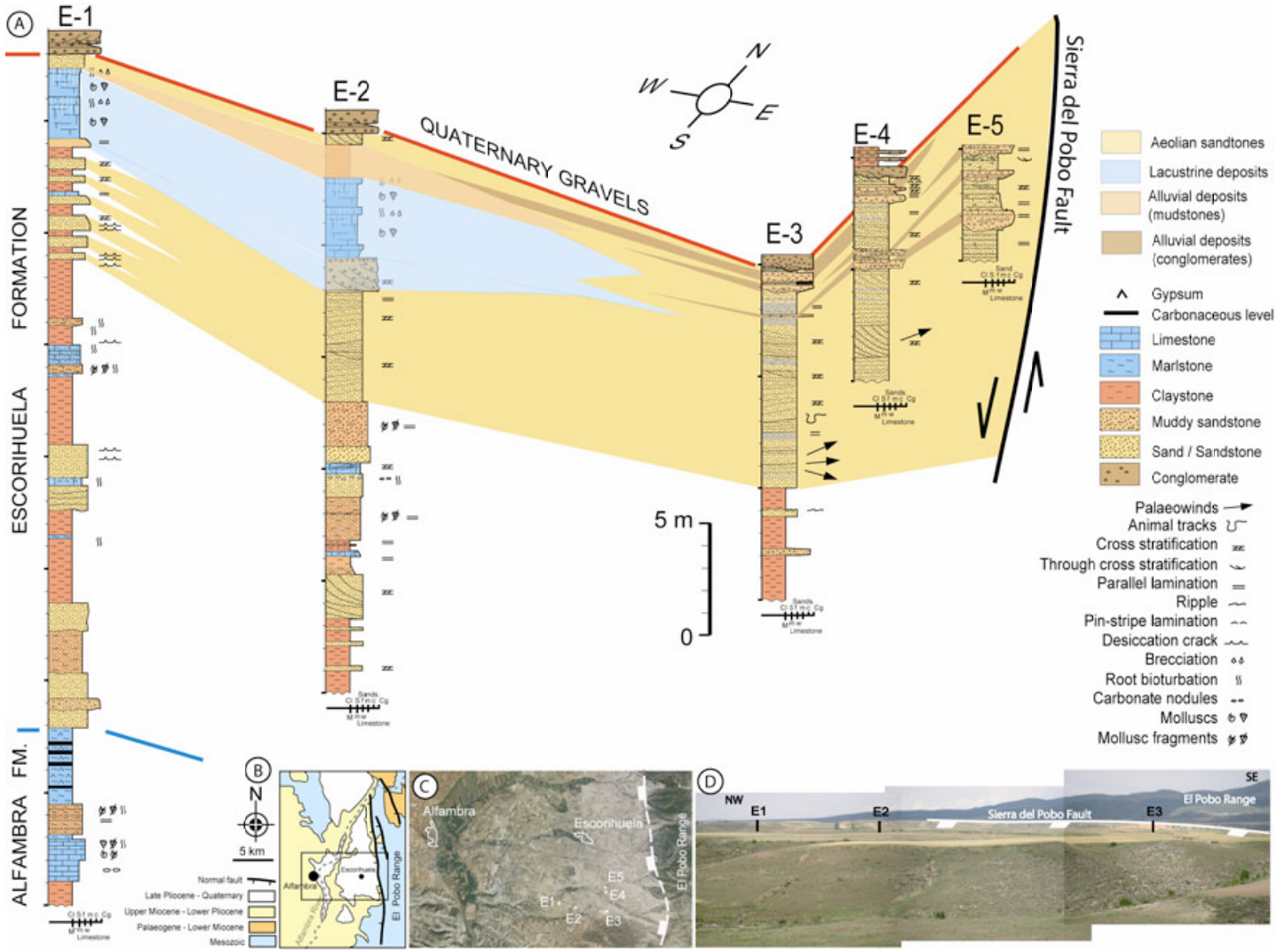
A
E-1
E-2
E-3
E-4
E-5
QUATERNARY GRAVELS
Sierra del Pobo Fault
N
W
E
S
5 m
0
ESCORIHUELA FORMATION
ALFAMBRA FM.
Aeolian sandtones
Lacustrine deposits
Alluvial deposits (mudstones)
Alluvial deposits (conglomerates)
Gypsum
Carbonaceous level
Limestone
Marlstone
Claystone
Muddy sandstone
Sand / Sandstone
Conglomerate
Palaeowinds
Animal tracks
Cross stratification
Through cross stratification
Parallel lamination
Ripple
Pin-stripe lamination
Desiccation crack
Brecciation
Root bioturbation
Carbonate nodules
Molluscs
Mollusc fragments
B
N
5 km
Normal fault
Late Pliocene - Quaternary
Upper Miocene - Lower Pliocene
Palaeogene - Lower Miocene
Mesozoic
Alfambra
Escorihuela
El Pobo Range
C
Alfambra
Escorihuela
E1
E2
E3
E4
E5
El Pobo Range
D
NW
SE
E1
E2
E3
Sierra del Pobo Fault
El Pobo Range

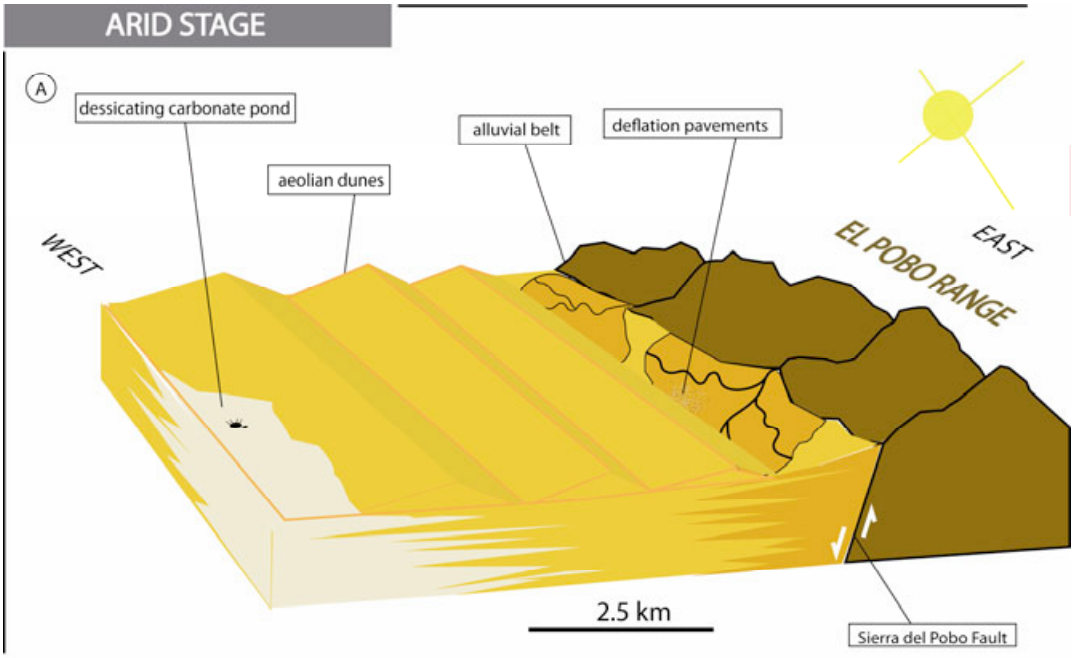
ARID STAGE
A
dessicating carbonate pond
aeolian dunes
alluvial belt
deflation pavements
WEST
EAST
EL POBO RANGE
2.5 km
Sierra del Pobo Fault

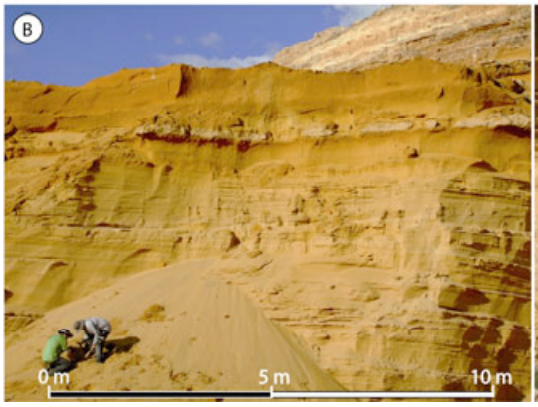
B
0 m
5 m
10 m

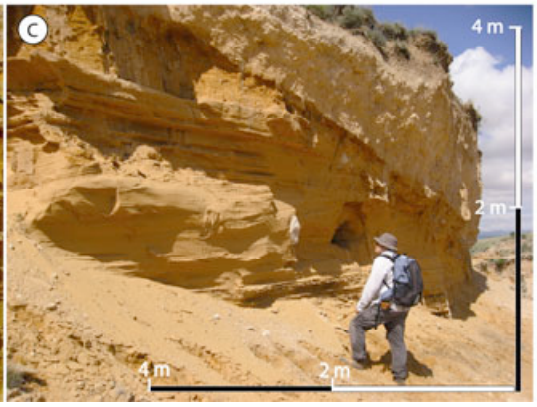
C
4 m
2 m
4 m
2 m

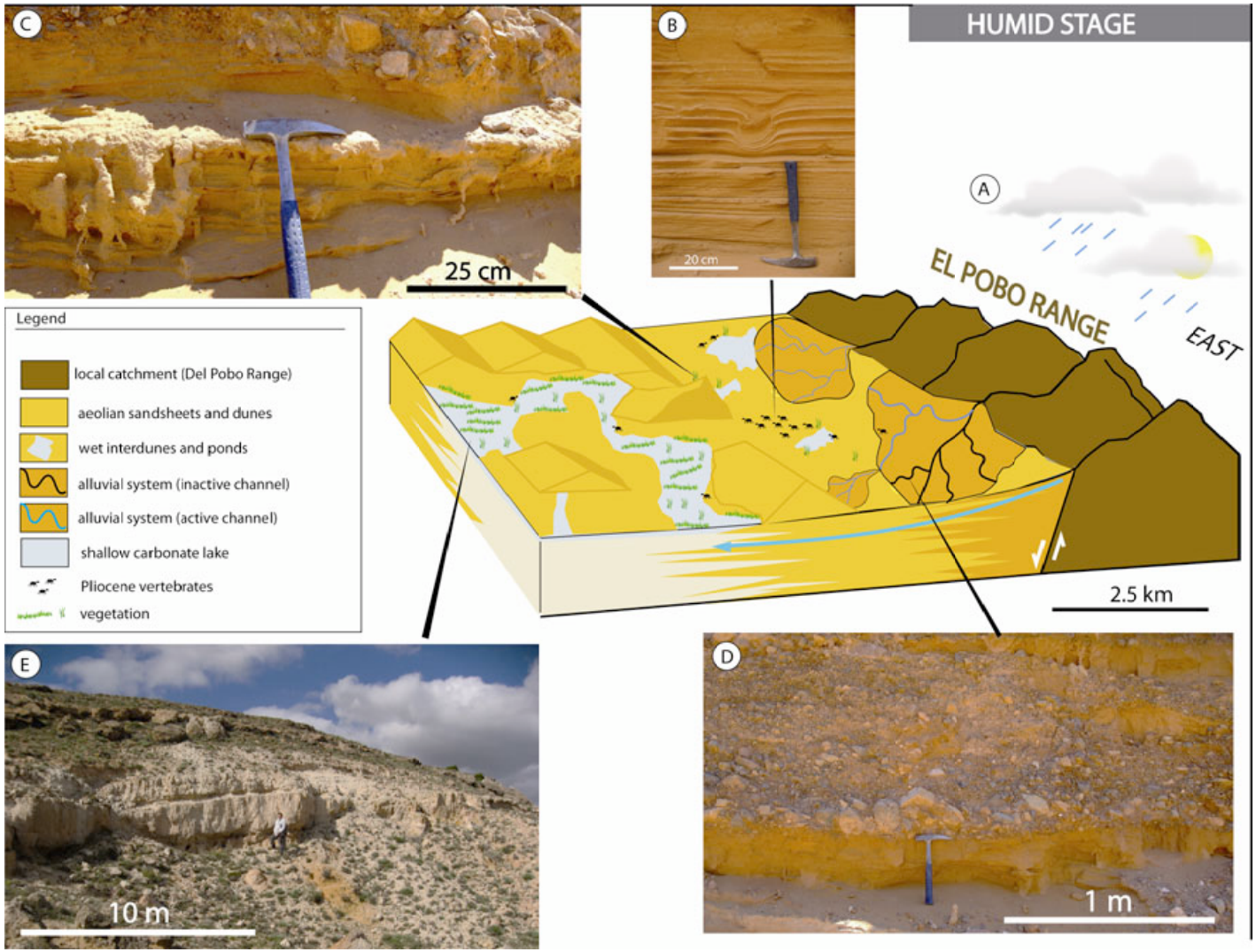
C
25 cm
B
20 cm
HUMID STAGE
A
EL POBO RANGE
EAST
Legend
local catchment (Del Pobo Range)
aeolian sandsheets and dunes
wet interdunes and ponds
alluvial system (inactive channel)
alluvial system (active channel)
shallow carbonate lake
Pliocene vertebrates
vegetation
2.5 km
E
10 m
D
1 m

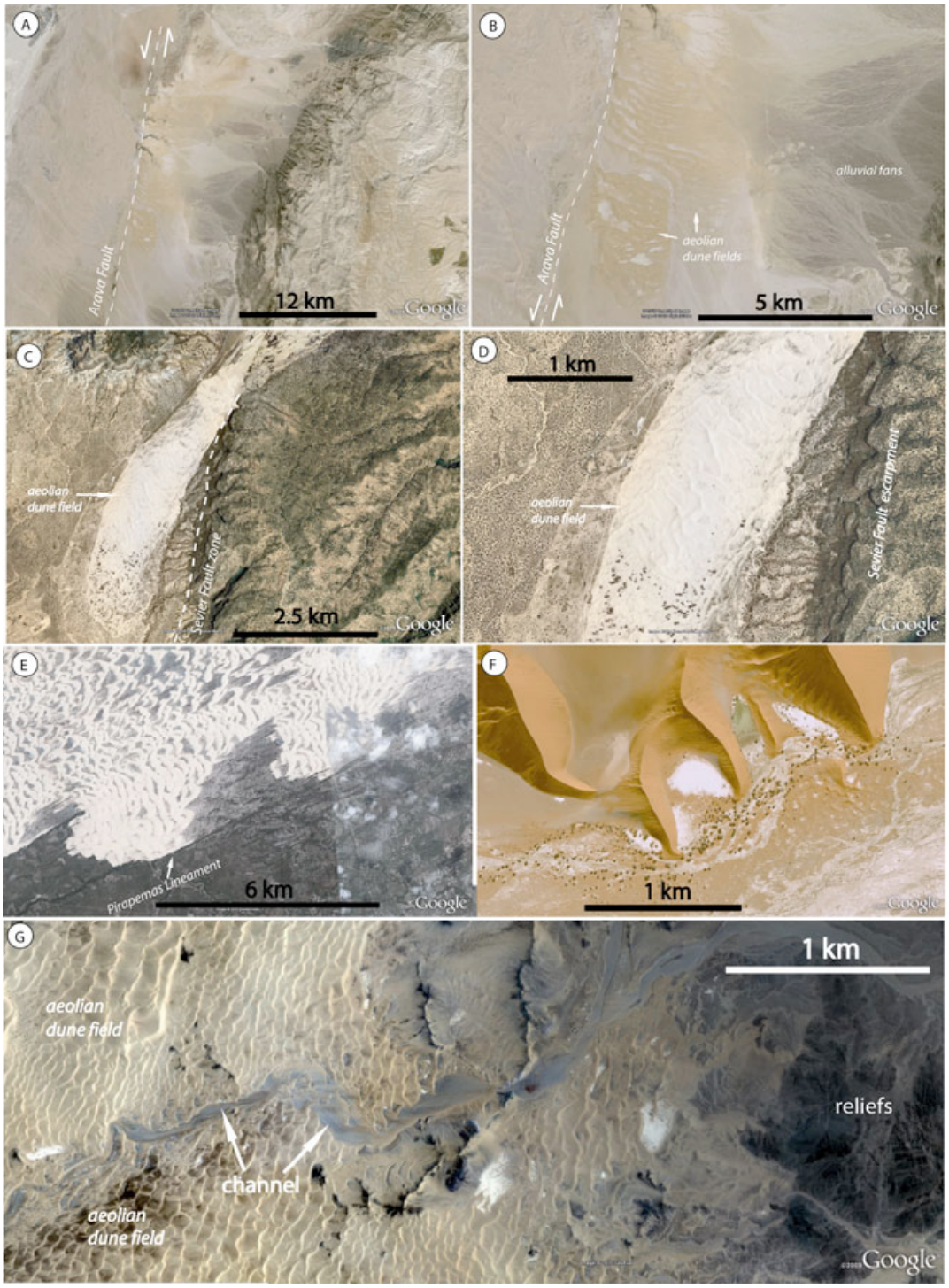
A
Arava Fault
12 km
Google
B
alluvial fans
aeolian
dune fields
Arava Fault
5 km
Google
C
aeolian
dune field
Sevier Fault zone
2.5 km
Google
D
1 km
aeolian
dune field
Sevier Fault escarpment
Google
E
Pirapemas Lineament
6 km
Google
F
1 km
Google
G
1 km
aeolian
dune field
reliefs
channel
aeolian
dune field
Google

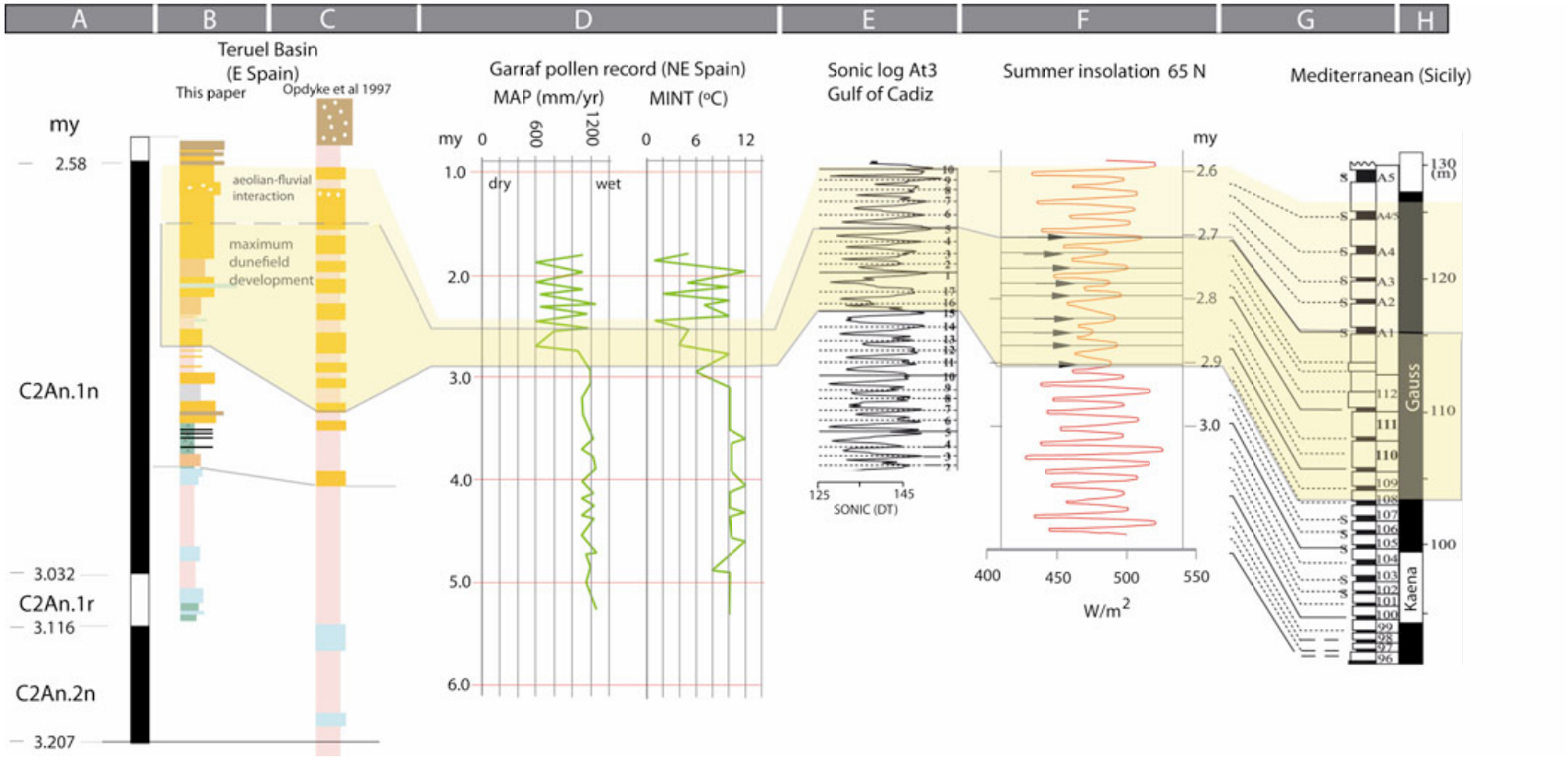
A
B
C
D
E
F
G
H
Teruel Basin
(E Spain)
This paper
Opdyke et al 1997
my
2.58
C2An.1n
3.032
C2An.1r
3.116
C2An.2n
3.207
aeolian-fluvial
interaction
maximum
dunefield
development
Garraf pollen record (NE Spain)
MAP (mm/yr)
MINT (ºC)
my
0
600
1200
0
6
12
1.0
2.0
3.0
4.0
5.0
6.0
dry
wet
Sonic log At3
Gulf of Cadiz
125
145
SONIC (DT)
Summer insolation 65 N
my
2.6
2.7
2.8
2.9
3.0
400
450
500
550
W/m2
Mediterranean (Sicily)
130
(m)
120
110
100
Gauss
Kaena